

UNIVERSITÉ DU QUÉBEC À MONTRÉAL

DIAGNOSTIC DE LA VARIABILITÉ INTERNE D'UN ENSEMBLE DE
SIMULATIONS DU MODÈLE RÉGIONAL CANADIEN DU CLIMAT

MÉMOIRE
PRÉSENTÉ
COMME EXIGENCE PARTIELLE
DE LA MAÎTRISE EN SCIENCES DE L'ATMOSPHÈRE

PAR

OUMAROU NIKIEMA

AVRIL 2010

UNIVERSITÉ DU QUÉBEC À MONTRÉAL
Service des bibliothèques

Avertissement

La diffusion de ce mémoire se fait dans le respect des droits de son auteur, qui a signé le formulaire *Autorisation de reproduire et de diffuser un travail de recherche de cycles supérieurs* (SDU-522 – Rév.01-2006). Cette autorisation stipule que «conformément à l'article 11 du Règlement no 8 des études de cycles supérieurs, [l'auteur] concède à l'Université du Québec à Montréal une licence non exclusive d'utilisation et de publication de la totalité ou d'une partie importante de [son] travail de recherche pour des fins pédagogiques et non commerciales. Plus précisément, [l'auteur] autorise l'Université du Québec à Montréal à reproduire, diffuser, prêter, distribuer ou vendre des copies de [son] travail de recherche à des fins non commerciales sur quelque support que ce soit, y compris l'Internet. Cette licence et cette autorisation n'entraînent pas une renonciation de [la] part [de l'auteur] à [ses] droits moraux ni à [ses] droits de propriété intellectuelle. Sauf entente contraire, [l'auteur] conserve la liberté de diffuser et de commercialiser ou non ce travail dont [il] possède un exemplaire.»

REMERCIEMENTS

La rédaction de ce mémoire a été rendue possible grâce au soutien continual de mon directeur de recherche, Monsieur René LAPRISE membre du Réseau Canadien en Modélisation et Diagnostics du Climat Régional. Je vous remercie Monsieur le Professeur pour m'avoir appuyé et donné l'opportunité de réaliser ce projet.

J'adresse un vif remerciement aux évaluateurs de ce mémoire, ainsi qu'à l'ensemble du corps professoral pour son immense appui. Mention spéciale à mes collègues et toute l'Équipe de Simulations Climatiques d'Ouranos, que je remercie.

Je ne saurais terminer sans mentionner mon épouse Hawa SAWADOGO et ma fille Sarah NIKIEMA pour leur soutien, sans oublier Ismael NIKIEMA pour ces sourires intermittents!!!!

TABLE DE MATIÈRES

LISTE DES FIGURES	v
LISTE DES ABREVIATIONS, SIGLES ET ACRONYMES	vii
LISTE DES SYMBOLES	viii
RÉSUMÉ	xi
ABSTRACT	xii
INTRODUCTION	1
CHAPITRE I	5
Abstract	7
1. Introduction	8
2. Equations for the time-evolution of the Internal Variability	10
2.1. The potential temperature IV equation	11
2.2. The relative vorticity IV equation	16
2.3. Domain, Simulation and Evaluation methods.....	19
3. Results and Analysis	21
3.1. Vertical profile and time evolution of the IV	21
3.2. Validation of the Internal Variability budget equation	24
3.3. Spatial patterns of the internal variability tendency.....	24
3.4. Time evolution of the domain-average internal variability tendency	25
3.4.1. Budget of the potential temperature IV	26

3.4.2. Budget of the relative vorticity IV	28
4. Conclusions	30
FIGURES	34
CONCLUSION	49
APPENDICES	54
RÉFÉRENCES	62

LISTE DES FIGURES

Figure	Page
1 (a, d) Vertical profile of time- and domain-averaged inter-member variance for the potential temperature and the relative vorticity. The 1050-hPa level is an extrapolation of the 1000-hPa level ; (b, c, e, f) time evolution of the domain average variance for the potential temperature and relative vorticity at different pressure levels.....	35
2 Time-averaged over 3-month period of the inter-member variance for the potential temperature (a, b, c) and the relative vorticity (d, e, f). The domain of interest is shown in Fig. 2a.....	36
3 Field of inter-member variance for the potential temperature at (A) 200 hPa and (B) 925 hPa, during the period of large increase of IV from 17 to 21 July (see Fig. 1c).....	37
4 Field of inter-member variance for the relative vorticity at (A) 300 hPa and (B) 925 hPa, during the period of the large increase of IV from 17 to 21 July (see Fig. 1f).....	38
5 Left-hand side term (L_θ) and the sum of all right-hand side terms (R_θ) of the potential temperature inter-member variance equation on certain dates of the period of interest at different pressure levels: (A) 200 hPa and (B) 925 hPa.....	39
6 Left-hand term (L_ζ) and the sum of all right-hand terms (R_ζ) of the relative vorticity inter-member variance equation during the period of interest at different pressure levels: (A) 300 hPa, (B) 925 hPa.....	40
7 Dispersion diagram of all grid points (except the sponge zone) to illustrate the comparison between the left-hand term and the sum of all right-hand terms at different pressure levels for the (A) potential temperature and the (B) relative vorticity.....	41

8	Time evolution of the left-hand term and the sum of all right-hand terms of the domain-averaged inter-member variance equations for the potential temperature (a, c) and the relative vorticity (b, d) at different pressure levels; (e, f) dispersion diagram to illustrate the comparison between these two sides of the equation.....	42
9	Vertical profiles of R different terms of the domain-averaged inter-member variance equation for the potential temperature (a, b, c) and the relative vorticity (d, e, f). The 1050-hPa level is an extrapolation of the 1000-hPa level.....	43
10	Time evolution of different terms on the right-hand side of domain-averaged inter-member variance equations for the potential temperature (a, b) and the relative vorticity (c, d, e, f) during the period of interest.....	44
11	Field of each term on the right-hand side of the inter-member variance equation for the potential temperature on 20 July 1993 at 0000 UTC at different pressure levels: (A) 200 hPa and (B) 925 hPa...	45
12	Fields of each term on the right-hand side of the inter-member variance equation for the relative vorticity on 20 July 1993 at 0000 UTC at different pressure levels: (A) 300 hPa, (B) 925 hPa.....	46
13	Time evolution of different parts in terms B_v (a, b) and C (e,f) of the potential temperature IV equation. Different fields show the covariance of fluctuations in B_v at (c) 400 hPa and (d) 850 hPa, and the covariance of fluctuation associated to (g) condensation (precipitation) and (h) convection in C at 400 hPa. Fields are valid on July, 19 at 0000 UTC.....	47
14	Time evolution of the covariance of fluctuation in B_h of the (A) potential temperature IV equation and the (B) relative vorticity IV equation. Different fields show the covariance of fluctuations in B_h at 925 hPa on July 19, 1993 at 0000 UTC.....	48

LISTE DES ABREVIATIONS, SIGLES ET ACRONYMES

CI	Conditions initiales
CRCM	Canadian Regional Climate Model
GCM	General Circulation Model
IC	Initial Conditions
IV	Internal Variability
LBC	Lateral Boundary Conditions
MCG	Modèle de Circulation Générale
MRC	Modèle Régional de Climat
MRCC	Modèle Régional Canadien du Climat
NCEP	National Centers for Environmental Prediction
RCM	Regional Climate Model
SST	Sea Surface Temperature
UQAM	Université du Québec à Montréal
US	United States
VI	variabilité interne

LISTE DES SYMBOLES

c	constante de diffusion horizontale
C_p	coefficient de chaleur spécifique à pression constante
f	paramètre de Coriolis
F_x	sources et puits de la quantité de mouvement pour la composante U du vent
F_y	sources et puits de la quantité de mouvement pour la composante V du vent
i	indice de points de grille dans la direction X
I	nombre total de point de grille dans la direction X
j	indice de points de grille dans la direction Y
J	nombre total de point de grille dans la direction Y
J_n	sources et puits de la température potentielle pour le membre n
k	indice de points de grille dans la direction Z
L_θ	tendance de la VI pour la température potentielle
L_ζ	tendance de la VI pour le tourbillon relatif
L_φ	tendance de la VI pour une variable quelconque φ
m	facteur d'échelle pour une projection stéréographique polaire
n	numéro du membre
N	nombre total de membre
p	pression
p_0	pression de référence
R	constante des gaz pour l'air sec
R_θ	somme de tous les termes de droit de l'équation de la VI pour la température potentielle
R_ζ	somme de tous termes de droit de l'équation de la VI pour le tourbillon

relatif

R_ϕ	somme de tous les termes de droite de l'équation de la VI pour une variable quelconque ϕ
S	terme de projection
t	temps
T	Température
u	composante du vent horizontal réel selon x
U_n	composante du vent horizontal modèle dans la direction X pour le membre n
v	composante du vent horizontal réel selon y
V_n	composante du vent horizontal modèle dans la direction Y pour le membre n
w	composante de la vitesse verticale selon z
x	coordonnée du référentiel cartésien local dans la direction est
X	coordonnée de la projection stéréographique polaire
y	coordonnée du référentiel cartésien local dans la direction nord
Y	coordonnée de la projection stéréographique polaire
z	coordonnée du référentiel cartésien local dans la direction verticale
$\overline{\langle \rangle}'$	opérateur de la moyenne temporelle
$\overline{\langle \rangle}^{xy}$	opérateur de la moyenne spatiale sur un domaine d'intérêt
$\langle \rangle$	opérateur de la moyenne d'ensemble
δ	opérateur différentiel
ζ	tourbillon relatif
θ	température potentielle
κ	coefficient de chaleur spécifique à pression constante (R/C_p)
λ	longitude
σ_ζ	variance ou VI pour le tourbillon relatif

σ_θ	variance ou VI pour la température potentielle
φ	variable atmosphérique quelconque
τ	nombre total d'archivage
ϕ	hauteur du geopotentiel
ψ	latitude
ψ_0	latitude de référence
ω	mouvement vertical selon p

RÉSUMÉ

Les Modèles Régionaux du Climat (MRC) ont longtemps été considérés comme des outils performants, de haute résolution à aire limitée permettant une meilleure compréhension du climat passé, présent et futur. Le plus souvent, les MRC sont pilotés à leurs frontières latérales par des Modèles Globaux du Climat (MGC) de basse résolution, et qui couvrent le reste du globe terrestre. Ces modèles ont la particularité de reproduire différentes solutions de l'état de l'atmosphère à cause de leur sensibilité aux conditions initiales (CI). Outre la solution due aux forçages externes (forçage aux frontières latérales et le forçage de surface), les MRC reproduisent une seconde solution associée à la variabilité interne (VI) du modèle du fait de leur sensibilité aux CI. Cette sensibilité est en grande partie causée par la nature non-linéaire de la physique et la dynamique atmosphériques.

À l'instar de précédentes études, nous analysons la variabilité interne du Modèle Régional Canadien du Climat (MRCC) en utilisant un ensemble de simulations aux CI différentes. Ce projet de recherche consiste à effectuer un diagnostic quantitatif des termes dynamique et diabatique qui contribuent à la variation temporelle et la distribution spatiale de la VI. L'originalité de ce travail est qu'il propose des équations bilans de la VI pour deux variables atmosphériques : la température potentielle et le tourbillon relatif. Les deux équations établies présentent des termes similaires, notamment les termes relatifs au transport de la VI par l'écoulement de la moyenne d'ensemble et la covariance des fluctuations agissant sur le gradient de la moyenne d'ensemble de la variable considérée.

Concrètement, nous avons utilisé un ensemble de 20 simulations aux CI différentes pour analyser les caractéristiques de la VI, afin de déterminer une période et une région d'intérêt caractérisées par une forte croissance de la VI. Ensuite, nous avons validé les équations établies en montrant l'égalité entre les deux parties de chaque équation. Enfin, une étude de bilan a permis d'évaluer la contribution des différents termes au développement et à l'évolution de la VI. Les résultats révèlent que les termes dominants responsables de l'accroissement de la VI sont soit les termes de covariance impliquant les fluctuations de température potentielle et de chauffage diabatique, ou les termes de covariance de fluctuations inter-membres agissent sur le gradient de la moyenne d'ensemble de la variable considérée. Les résultats révèlent également que les épisodes de fortes diminutions de la VI se produisent lorsque les maxima de la VI sont proches de la frontière nord-est, indiquant leur transport en dehors de la zone d'étude par l'écoulement moyen. Enfin, nos résultats ont montré qu'en moyenne, les termes du troisième ordre sont négligeables, mais peuvent devenir importants lorsque la VI est importante.

Mots clés : Équation de la variabilité interne, modèle régional de climat, ensemble de simulations, climat de l'Amérique du Nord.

ABSTRACT

The regional climate models (RCM) have long been considered as powerful tools that allow better understanding of climate, because of their high resolution on limited areas. Most often, the RCM are driven at their lateral boundaries by a low resolution model (Global Climate Models, GCM), which covers the entire earth. These models have a particularity to reproduce different solutions of the atmospheric state due to their sensitivity to initial conditions (IC). Besides the solution resulting from external forcing, the MRC reproduce other solution associated with internal variability (IV) due to their sensitivity to IC. This sensitivity is caused by the chaotic and nonlinear nature of the atmospheric dynamics.

As in like previous studies, we analyze the Canadian RCM internal variability using an ensemble of simulations run with different IC. This project performs a quantitative diagnostic of dynamic and diabatic terms that contribute to the temporal variation of IV. The originality of this work is that it proposes budget equations of the IV of two atmospheric variables: potential temperature and relative vorticity. For both of these variables, the IV equations present similar terms, notably terms relating to the transport of IV by ensemble-mean flow and to the covariance of fluctuations acting on the gradient of the ensemble-mean state.

In practice, we used a set of 20-member set of simulations that differ only in their IC to analyze the IV characteristics. We identify a period and an area of interest characterized by large IV variations. Then, we show the skill of these equations to diagnose the IV by comparing both sides of each equation. Finally, we assess the quantitative contribution of each term to the IV tendency. Our study suggests that the dominant terms responsible for the large increase of IV are either the covariance term involving the potential temperature fluctuations and diabatic heating fluctuations, or the covariance of inter-member fluctuations acting upon ensemble-mean gradients. Results also reveal that the episodes of large decreases of IV occur when the maximum of IV are close to the northeast boundary, and eventually get transported out of the regional domain by the ensemble-mean flow. Finally, our results reveal that, on average, the third-order terms are negligible, but they can become important when the IV is large.

Keywords: internal variability equation, – Regional climate models – Ensemble of simulations – North American climat

INTRODUCTION

L'atmosphère est constituée d'un fluide qui obéit aux principes fondamentaux de la mécanique des fluides et de la thermodynamique. Elle est caractérisée par plusieurs paramètres tels que la température, la pression, l'humidité, la teneur en eau liquide et la vitesse (horizontale et verticale) de l'air. L'évolution de tous ces paramètres peut être suivie en utilisant leur équation d'évolution respective. Ainsi, les prévisions climatiques à court, moyen et long terme sont faites grâce aux modèles numériques basés sur certaines lois de la physique, notamment les lois thermodynamiques, de conservation de la masse et les équations d'Euler qui décrivent l'évolution d'un fluide à la surface d'une sphère en rotation.

De nos jours, à cause de leurs performances et de leurs capacités à reproduire les processus physiques de l'atmosphère avec une haute résolution, les Modèles Régionaux du Climat (MRC) sont utilisés pour simuler le climat passé, présent et futur. Les MRC sont intégrés sur un domaine à aire limitée avec des conditions initiales (CI) et des conditions frontières latérales (CFL) fournies par un modèle de circulation générale (MCG) ou par des données de ré-analyses. Le pilotage unidirectionnel du MCG vers le MRC consiste en une transmission d'informations de la grande échelle vers la petite échelle, rendant ainsi possible le calcul à haute résolution.

À l'instar des modèles de circulations générales, les MRC sont sensibles aux CI en raison du caractère non-linéaire de la dynamique atmosphérique (Lorenz 1963); cependant les CFL exercent une contrainte qui limite le degré de liberté des modèles pilotés. Il est maintenant démontré que les MRC développent un certain degré de variabilité interne (VI. défini comme étant la différence qui existe entre les simulations exécutées avec différentes CI) en raison des non-linéarités de la physique et de la dynamique du modèle (Weisse et al. 2000; Giorgi et Bi 2000; Rinke et Dethloff 2000, Christensen et al. 2001; Caya et Biner 2004; Rinke et al 2004; Alexandru et al. 2007; Lucas-Picher et al. 2008).

Dans leurs simulations réalisées sur un domaine couvrant l'est de l'Asie, Giorgi et Bi (2000) ont montré que la VI du modèle est maximale en été et très faible en hiver. La forte VI en été serait liée aux non-linéarités associées aux processus de convection et de précipitations, alors qu'en hiver, le fort courant jet d'ouest réduit la variabilité du modèle en raison des intenses forçages exercés aux frontières latérales. Un important résultat de leur étude est que la VI semble être liée aux régimes saisonniers et synoptiques.

Dans leur étude sur un domaine de l'Arctique, Rinke et Dethloff (2000) et Rinke et al. (2004) ont montré que le contrôle exercé par les CFL est plus faible comparé aux domaines de moyenne latitude. Ils ont constaté que la VI est importante en automne/hiver, et faible en été. Ce résultat est une conséquence de la circulation particulière de l'Arctique et de l'activité des ondes planétaires qui sont faibles en été.

Christensen et al. (2001) ont porté une attention à la variabilité interne en comparant les simulations de deux MRC réalisées sur une même zone méditerranéenne. Ils ont constaté que la VI du modèle dépend du type de variable étudié, des caractéristiques du modèle, ainsi que de la zone d'intégration. Toutefois, les intensités de la variabilité sont d'un ordre de grandeur comparable pour les deux modèles. Leur étude a également montré l'impact de la VI sur la précision des résultats du MRC.

Caya et Biner (2004) ont étudié la VI dans les simulations du Modèle Régional Canadien du Climat (MRCC) sur un domaine couvrant l'est de l'Amérique du Nord et une partie de l'océan Atlantique. Comme Giorgi et Bi (2000), ils ont trouvé de faibles intensités de la VI en hiver, au printemps et en automne, et de forte intensité en été, de sorte que les simulations seraient parfois différentes pour les mêmes situations météorologiques. Lucas-Picher et al. (2004, 2008) ont constaté que, pour une saison donnée, l'ordre de grandeur de la VI est directement lié à la taille du domaine. Contrairement aux études précédentes, ils ont constaté une importante VI en hiver pour un domaine suffisamment grand.

Récemment, Alexandru et al. (2007) ont étendu les études antérieures avec le MRCC sur le domaine de l'Amérique du Nord en utilisant un ensemble de 20 simulations réalisées pour la saison de l'été 1993. Leurs résultats montrent que durant l'intégration l'intensité de la VI varie fortement avec les événements synoptiques. La répartition géographique de la VI dépend des variables étudiées. Les fortes précipitations dans le sud des États-Unis semblent agir comme un mécanisme déclencheur de la VI pour la hauteur du géopotentiel à 850 hPa. Celle-ci se développe le long des trajectoires des tempêtes et elle atteint son maximum dans la partie nord-est de la région d'étude.

Les travaux antérieurs ont mis en évidence la présence de VI dans les simulations des MRC, toutefois leur intensité est faible comparée à celle des modèles de circulations globales à cause du contrôle exercé aux frontières latérales. Les mécanismes physiques responsables du développement épisodique de la VI semblent être difficile à élucider. Certaines hypothèses ont été émises sur ces mécanismes qui favorisent le déclenchement de forte VI, notamment les non-linéarités associées à la transmission d'information de la grande échelle vers les petites échelles, les non-linéarités associées aux processus de paramétrisation diabatique telle que la condensation et la convection, les instabilités hydrodynamiques associées aux forts gradient de température et du vent. Ce projet vise à approfondir notre compréhension du processus de développement de la VI en effectuant un diagnostic quantitatif des différentes contributions à la variation temporelle et la distribution spatiale de la VI. Dans la section 2 de l'article de ce mémoire, nous présentons la méthodologie utilisée pour établir les équations bilans de la VI pour la température potentielle et le tourbillon relatif. Dans la section 3, nous présentons les différents résultats obtenus en utilisant une base de données issue des travaux d'Alexandru et al. (2007). Nous commençons par étudier les caractéristiques de la VI de l'ensemble des simulations réalisées avec différentes CI. Ensuite, nous étudions la validité de ces équations en vérifiant l'égalité entre les deux parties de chaque équation. Enfin, l'analyse des différentes contributions à la tendance de la VI fera la lumière sur les mécanismes

physiques sous-jacents au développement de la VI. Les principales conclusions seront résumées dans la section 4.

CHAPITRE I

DIAGNOSTIC DE LA VARIABILITÉ INTERNE D'UN ENSEMBLE DE SIMULATIONS DU MODÈLE RÉGIONAL CANADIEN DU CLIMAT

Ce chapitre, présenté sous forme d'un article rédigé en anglais, présente un diagnostic quantitatif des différentes contributions diabatique et dynamique à la variation temporelle et la distribution spatiale de la VI. Des équations bilans de la VI pour la température potentielle et le tourbillon relatif ont été établies. Puis, l'utilisation d'un ensemble de simulations du MRCC a permis d'effectuer une étude de validation de ces équations. Enfin, une étude bilan a été réalisée dans le but d'identifier les mécanismes physiques sous-jacents au développement de la VI. Par ailleurs, le chapitre fournit des informations sur le MRCC, la base de données utilisées et la méthodologie appliquée.

**Diagnostic budget study of the Internal Variability in ensemble simulations of
the Canadian RCM**

Oumarou NIKIEMA * and René LAPRISE

Canadian Network for Regional Climate Modelling and Diagnostics, Centre
ESCER, UQAM, B.P. 8888, Stn Downtown, Montreal, QC, Canada H3C 3P8

* Corresponding author's address:

Oumarou Nikiema,
Département des Sciences de la Terre et de l'Atmosphère,
UQAM, ESCER, Département des Sciences de la Terre et de l'Atmosphère, UQAM,
B.P. 8888, Stn Downtown, Montreal, QC, Canada H3C 3P8
E-mail : nikiema@sca.uqam.ca

Abstract

Due to the chaotic and nonlinear nature of the atmospheric dynamics, it is known that small differences in the initial conditions (IC) of models can grow and affect the simulation evolution. In this study, we perform a quantitative diagnostic budget calculation of the various diabatic and dynamical contributions to the time evolution and spatial distribution of internal variability (IV) in simulations with the nested Canadian Regional Climate Model. We establish prognostic budget equations of the IV for the potential temperature and the relative vorticity fields. For both of these variables, the IV equations present similar terms, notably terms relating to the transport of IV by ensemble-mean flow and to the covariance of fluctuations acting on the gradient of the ensemble-mean state. We show the skill of these equations to diagnose the IV that took place in an ensemble of 20 three-month (summer season) simulations that differed only in their IC. Our study suggests that the dominant terms responsible for the large increase of IV are either the covariance term involving the potential temperature fluctuations and diabatic heating fluctuations, or the covariance of inter-member fluctuations acting upon ensemble-mean gradients. Our results also show that, on average, the third-order terms have little contribution, but they can become important when the IV is large.

Keywords: Internal variability equations – Regional climate models – Ensemble of simulations – North American climate

1. Introduction

Nowadays, Regional Climate Models (RCM) are used to make retrospective climate simulations and future climate projections that include realistic weather sequences due to their capacity of representation of the physical processes with high resolution. RCM are integrated on a limited domain with initial conditions (IC) and lateral boundary conditions (LBC) provided either by an archived simulation of a driving global model (such as Coupled Global Climate Model) or by gridded analyses of observations. The dynamical downscaling paradigm consists of the transmission of information from large to small scales, as well as fine-scale forcings permitted by the use of high-resolution computational grids.

Global atmospheric models are sensitive to IC because of the nonlinear nature of the atmospheric dynamic (Lorenz 1963). Similar processes operate in RCMs; LBC however exert a constraint that limits the degrees of freedom of the nested simulations. It is now documented that RCM exhibit a certain level of internal variability (IV, defined as the difference between members in an ensemble of simulations that differ only in their IC) due in part to nonlinearities in the model physics and dynamics (Weisse et al. 2000; Giorgi and Bi 2000; Rinke and Dethloff 2000; Christensen et al. 2001; Caya and Biner 2004; Rinke et al. 2004; Alexandru et al. 2007; Lucas-Picher et al. 2008).

In their simulations over eastern Asia, Giorgi and Bi (2000) have shown that RCMs' IV is maximum in summer, and it becomes very weak in the winter. The large IV in summer appears related to local and intermittent processes such as convection and precipitation processes, whereas in winter, the westerly flow sweeps away internally generated variability. An important result of their study is that the IV appears sensitive to seasonal and synoptic regimes.

In their study over an Arctic domain, Rinke and Dethloff (2000) and Rinke et al. (2004) showed that the LBC control is weaker compared to mid-latitude domains. They found large IV in autumn/winter and small IV in summer, which they explained

as a consequence of the Arctic circulation and synoptic activity being weaker in summer.

Caya and Biner (2004) studied IV in simulations of the Canadian RCM (CRCM) over a domain covering the eastern North America and a part of the Atlantic Ocean. Like Giorgi and Bi (2000), they found small IV in winter and most of spring and autumn, and much larger IV in summer, so that the simulations would occasionally diverge toward different meteorological situations. Lucas-Picher et al. (2004, 2008) found that, for a given season, the magnitude of IV directly scales with domain size. Unlike previous studies, they found IV to be largest in winter with a sufficiently large domain.

Alexandru et al. (2007) extended the previous work with CRCM using an ensemble with 20 members for the summer season over eastern North America with various domain sizes. Their results show that the IV magnitude strongly fluctuates with synoptic events during the simulations, and the geographical distribution of IV changes with variables. The strong precipitation events in the southern United States appear to act as a triggering mechanism for the 850-hPa geopotential IV, which continues to develop along the storm track and reaches its maximum toward the north-east of the study domain.

Previous work has documented the occurrence of IV in RCM. The LBC exerts a control that contribute to generally maintaining IV's magnitude below the value prevailing in simulations with global models, which equals transient-eddy amplitude. The exact mechanisms responsible for the episodic development of IV in RCM remain elusive however. A mixture of trigger mechanisms have been hypothesised, including the interaction of large-scale flow with fine-scale surface inhomogeneities, the stochastic behaviour of parameterised diabatic effects such as convection and condensation, the cascade of information from the large to small scales through the nonlinear processes of shearing-folding-twisting-tilting, and hydrodynamic instabilities associated with strong temperature gradients and wind shears.

This paper aims at furthering our understanding of the IV development process by performing a quantitative diagnostic calculation of the various diabatic and dynamic contributions to the temporal variation and spatial distribution of IV. In Section 2 we will establish a prognostic equation of IV for potential temperature and relative vorticity. Then in Section 3, we will verify the skill of these equations at reproducing diagnostically, using only 6-hourly samples of model-simulated data interpolated on a predefined set of pressure levels, the IV that developed in the 20 simulations of Alexandru et al. (2007). Although such ensemble may seem small in comparison with the size of ensemble used for Numerical Weather Prediction, 20 members is, to our knowledge, the largest such ensemble having been used in the context of climate. The decomposition of the various contributions to the IV tendency will shed light on the underlying physical mechanism to the development of IV in RCM simulations. The main conclusions will be summarized in Section 4.

2. Equations for the time-evolution of the Internal Variability

This section describes the methodology used to establish the IV budget. We assume that we have available an archive of an ensemble of N member simulations over a given domain, all driven with the same lateral boundary conditions and the same model parameters (spatial and time resolution), the simulations differing only by the time of the start of each run. The first step to develop the IV budget equation consists in writing the basic equations solved by the CRCM, and thus by each member in the ensemble of CRCM simulations. We then combine these to form one equation for the potential temperature and one for the relative vorticity, the diabatic and dynamic variables that we picked to carry our diagnostic budget study. In step 2 we apply the ensemble-averaging operator to these equations, and in step 3, we subtract the equation of step 1 from the corresponding ones of the step 2 to get the equations for the deviation (or departures) from the ensemble-mean. In step 4, we multiply these equations by the deviation quantities, and apply ensemble-averaging operator to obtain prognostic equations of the inter-member variance. The final step

consists in comparing the prediction of these inter-member variance budget equations with the ensemble-mean of the square of the departures of the 20 members in the archived ensemble of CRCM simulations for the corresponding variables.

We chose to carry our diagnostic budget study in pressure coordinates for two reasons. First, by the physical interpretation of the various dynamical contributions is more easily made than in the terrain-following coordinates used to solve the model equations. Second, by the archived CRCM-simulated data were only available to us after their interpolation in pressure coordinates. Sections 2.1 and 2.2 describe in details these different steps to get the IV budget equations for potential temperature and relative vorticity, respectively.

2.1. The potential temperature IV equation

The internal variability is examined using an ensemble of N members of simulations that are differing only in their IC. For each member n , we write each model variable as $\varphi_n(i, j, k, t)$ that denotes the value of the variable at a position (i, j, k) and at time t . The first law of thermodynamics as resolved by the CRCM is formally equivalent to the following equation for potential temperature, when written on isobaric (p) surfaces:

$$\frac{d\theta_n}{dt} \equiv \frac{\partial\theta_n}{\partial t} + \vec{V}_n \cdot \vec{\nabla}\theta_n + \omega_n \frac{\partial\theta_n}{\partial p} = J_n \quad (1)$$

where $\theta_n = T_n \left(\frac{p_0}{p} \right)^\kappa$ is the potential temperature that a parcel of dry air at pressure p and temperature T would have if it were expanded or compressed adiabatically to a standard pressure p_0 (usually taken to be 1000 hPa). $\kappa = R/c_p$ is a constant, with R the gas constant for dry air and c_p the specific heat of dry air at constant pressure. $\vec{V}_n \equiv (U_n, V_n)$ is the horizontal wind image in polar stereographic

coordinates, defined in terms of the (u, v) horizontal wind components expressed in a Cartesian reference frame (x, y, z) with zonal and meridional orientation. ω_n ($\equiv \frac{dp}{dt}$) is the pressure vertical motion. $\bar{\nabla}$ is the lateral gradient operator evaluated on a surface of constant pressure. J_n represents total sources/sinks terms (diabatic heating rate). It regroups these five contributions: radiative heating rate, vertical diffusion heating rate, latent heat release rate, convective heating rate and the heating rate associated to the lateral diffusion. This last term is not archived as CRCM data; so it will be evaluated using its approximate contribution expressed as: $-c\nabla^4\theta$, where $c = 1.85 \times 10^{13} m^4 s^{-1}$ is the diffusion constant used in the 45-km version of the CRCM (Laprise et al. 1998).

Using the mass-continuity equation in vertical pressure coordinate, the Eq. 1 can be rewritten into flux form as:

$$\frac{\partial \theta_n}{\partial t} + \bar{\nabla} \cdot (\theta_n \bar{V}_n) + \frac{\partial (\theta_n \omega_n)}{\partial p} = J_n \quad (2)$$

According to the Reynolds decomposition, we suppose that each variable $\varphi_n \in \{\theta_n, U_n, V_n, \omega_n, J_n\}$ can be split in two parts: mean part that represents the ensemble-mean of the variable ($\langle \varphi \rangle$) and the difference (φ'_n) between each member variable and the ensemble-mean. So each member variable is defined as:

$$\varphi_n = \langle \varphi \rangle + \varphi'_n \quad (3)$$

where the ensemble-mean of the variable φ_n is estimated as:

$$\langle \varphi \rangle = \frac{1}{N} \sum_{n=1}^N \varphi_n \quad (4)$$

The internal variability is estimated using the approach of Alexandru et al. (2007), i.e. by calculating the inter-member variance σ_φ^2 of the variable φ_n approximated as the mean of the deviation square:

$$\sigma_{\varphi}^2(i, j, k, t) \approx \frac{1}{N} \sum_{n=1}^N \varphi_n'^2(i, j, k, t) \equiv \langle \varphi_n'^2 \rangle(i, j, k, t) \quad (5)$$

In this study, we used the biased variance estimator to evaluate the IV because with 20 members, the relative error is only 5%, which is less than the error introduced by several other approximations that will have to be made to complete the calculations.

We apply ensemble averaging $\langle \cdot \rangle$ to Eq. 2 to get the ensemble-mean prognostic equation of the potential temperature $\langle \theta \rangle$, as given by:

$$\frac{\partial \langle \theta \rangle}{\partial t} + \bar{\nabla} \cdot \langle \theta \bar{V} \rangle + \frac{\partial \langle \theta \omega \rangle}{\partial p} = \langle J \rangle \quad (6)$$

The deviation prognostic equation of the potential temperature is obtained by taking the difference between Eq. 2 and Eq. 6:

$$\frac{\partial \theta'_n}{\partial t} + \bar{\nabla} \cdot \left(\theta_n \bar{V}_n - \langle \theta \bar{V} \rangle \right) + \frac{\partial (\theta_n \omega_n - \langle \theta \omega \rangle)}{\partial p} = J'_n \quad (7)$$

By using the Reynolds decomposition of the product (see *Appendix A*), we can rewrite Eq. 7 as:

$$\begin{aligned} \frac{\partial \theta'_n}{\partial t} + \bar{V}'_n \cdot \bar{\nabla} \langle \theta \rangle + \langle \theta \rangle \bar{\nabla} \cdot \bar{V}'_n + \langle \bar{V} \rangle \cdot \bar{\nabla} \theta'_n + \theta'_n \bar{\nabla} \cdot \langle \bar{V} \rangle + \langle \theta \rangle \frac{\partial \omega'_n}{\partial p} + \omega'_n \frac{\partial \langle \theta \rangle}{\partial p} + \langle \omega \rangle \frac{\partial \theta'_n}{\partial p} + \theta'_n \frac{\partial \langle \omega \rangle}{\partial p} \\ + \bar{\nabla} \cdot \left(\theta'_n \bar{V}'_n - \langle \theta'_n \bar{V}'_n \rangle \right) + \frac{\partial}{\partial p} (\theta'_n \omega'_n - \langle \theta'_n \omega'_n \rangle) = J'_n \end{aligned} \quad (8)$$

Because the mass-continuity equation is linear, its ensemble-mean and deviation parts are readily obtained as:

$$\bar{\nabla} \cdot \langle \bar{V} \rangle + \frac{\partial \langle \omega \rangle}{\partial p} = 0 \quad (9)$$

$$\bar{\nabla} \cdot \bar{V}'_n + \frac{\partial \omega'_n}{\partial p} = 0 \quad (10)$$

Using these two last equations, Eq. 8 can be reduced to get the deviation equation as:

$$\begin{aligned} \frac{D\theta'_n}{Dt} &\equiv \frac{\partial\theta'_n}{\partial t} + \langle \bar{V} \rangle \cdot \bar{\nabla} \theta'_n + \langle \omega \rangle \frac{\partial\theta'_n}{\partial p} = -\bar{V}'_n \cdot \bar{\nabla} \langle \theta \rangle - \omega'_n \frac{\partial \langle \theta \rangle}{\partial p} - \bar{\nabla} \cdot (\theta'_n \bar{V}'_n - \langle \theta'_n \bar{V}'_n \rangle) \\ &\quad - \frac{\partial}{\partial p} (\theta'_n \omega'_n - \langle \theta'_n \omega'_n \rangle) + J'_n \end{aligned} \quad (11)$$

where $\frac{D}{Dt} = \frac{\partial}{\partial t} + \langle \bar{V} \rangle \cdot \bar{\nabla} + \langle \omega \rangle \frac{\partial}{\partial p}$

Multiplying Eq. 11 by θ'_n , we get:

$$\begin{aligned} \frac{\partial}{\partial t} \left[\frac{\theta'^2_n}{2} \right] + \frac{\langle \bar{V} \rangle}{2} \cdot \bar{\nabla} \theta'^2_n + \frac{\langle \omega \rangle}{2} \frac{\partial \theta'^2_n}{\partial p} &= -\theta'_n \bar{V}'_n \cdot \bar{\nabla} \langle \theta \rangle - \theta'_n \omega'_n \frac{\partial \langle \theta \rangle}{\partial p} \\ &\quad - \underbrace{\theta'_n \left[\bar{\nabla} \cdot (\theta'_n \bar{V}'_n - \langle \theta'_n \bar{V}'_n \rangle) + \frac{\partial}{\partial p} (\theta'_n \omega'_n - \langle \theta'_n \omega'_n \rangle) \right]}_{\text{Third-order terms}} + \theta'_n J'_n \end{aligned} \quad (12)$$

Finally, by applying ensemble averaging $\langle \rangle$ onto Eq. 12, we obtain the variance prognostic equation for potential temperature:

$$\begin{aligned} \frac{1}{2} \frac{D\sigma_\theta^2}{Dt} &\equiv \frac{\partial}{\partial t} \left[\frac{\sigma_\theta^2}{2} \right] + \langle \bar{V} \rangle \cdot \bar{\nabla} \frac{\sigma_\theta^2}{2} + \langle \omega \rangle \frac{\partial}{\partial p} \left[\frac{\sigma_\theta^2}{2} \right] = -\langle \theta'_n \bar{V}'_n \rangle \cdot \bar{\nabla} \langle \theta \rangle - \langle \theta'_n \omega'_n \rangle \frac{\partial \langle \theta \rangle}{\partial p} \\ &\quad - \langle \theta'_n \bar{\nabla} \cdot (\theta'_n \bar{V}'_n) \rangle - \left\langle \theta'_n \frac{\partial}{\partial p} (\theta'_n \omega'_n) \right\rangle + \langle \theta'_n J'_n \rangle \end{aligned} \quad (13)$$

where $\sigma_\theta^2 = \langle \theta'^2 \rangle$.

Operating with $\left[(13) + 1/2 \sigma_\theta^2 (9) \right]$, we get

$$L_\theta = R_\theta = A_h + A_v + B_h + B_v + C + E_h + E_v \quad (14)$$

where

$$\begin{aligned}
L_\theta &= \frac{\partial \sigma_\theta^2}{\partial t}; \\
A_h &= -\bar{\nabla} \cdot (\langle \bar{V} \rangle \sigma_\theta^2); \quad A_v = -\frac{\partial (\langle \omega \rangle \sigma_\theta^2)}{\partial p} \\
B_h &= -2 \langle \theta'_n \bar{V}'_n \rangle \cdot \bar{\nabla} \langle \theta \rangle; \quad B_v = -2 \langle \theta'_n \omega'_n \rangle \frac{\partial \langle \theta \rangle}{\partial p} \\
C &= 2 \langle \theta'_n J'_n \rangle; \\
E_h &= -2 \left\langle \theta'_n \bar{\nabla} \cdot (\theta'_n \bar{V}'_n) \right\rangle; \quad E_v = -2 \left\langle \theta'_n \frac{\partial}{\partial p} (\theta'_n \omega'_n) \right\rangle
\end{aligned}$$

The term L_θ is the diagnostic potential temperature IV tendency, which we will compare to the local changes of the inter-member spread variance in the archived ensemble of CRCM simulations, which will be referred to as the “left-hand side” in the following. There are four main terms on the right-hand side (R_θ): $A \equiv A_h + A_v$, $B \equiv B_h + B_v$, C and $E \equiv E_h + E_v$. The term A is a transport term describing the convergence of the potential temperature IV by the ensemble-mean flow; it is made up of contributions A_h and A_v from horizontal and vertical transports, respectively. The term B is a conversion term representing the covariance of potential temperature and flow fluctuations in the direction of the ensemble-mean potential temperature gradient; this term is also made of horizontal (B_h) and vertical (B_v) contributions, associated with the horizontal and vertical flow fluctuations and corresponding components of the ensemble-mean potential temperature gradient, respectively. The term C is generation (or diabatic source/sink) term arising from the covariance of fluctuations of potential temperature and diabatic heating rate; it includes contributions from radiation heating, latent heat release, convective heating, boundary layer heating, turbulent vertical diffusion, and lateral diffusion. The term E represents the third-order terms of the IV prognostic equation; it is the covariance of the potential temperature fluctuations and divergence of potential temperature flux due to fluctuations.

2.2. The relative vorticity IV equation

In the horizontal polar stereographic and the isobaric coordinates (X, Y, p), the relative vorticity (ζ) equation (see details in the *Appendix B*) can be written as:

$$\frac{d\zeta_n}{dt} \equiv \frac{\partial \zeta_n}{\partial t} + \bar{\nabla} \cdot (\zeta_n \bar{V}_n) + \omega_n \frac{\partial \zeta_n}{\partial p} = -\bar{\nabla} \cdot (f \bar{V}_n) + S \left[\frac{\partial \omega_n}{\partial Y} \frac{\partial U_n}{\partial p} - \frac{\partial \omega_n}{\partial X} \frac{\partial V_n}{\partial p} \right] + S \left[\frac{\partial F_{Yn}}{\partial X} - \frac{\partial F_{Xn}}{\partial Y} \right] - c \nabla^4 \zeta_n \quad (15)$$

where $S \equiv m^2 = (1 + \sin \psi_0)/(1 + \sin \psi)$ is the metric projection term for a polar stereographic projection; ψ and ψ_0 are latitude and reference latitude respectively; f is the Coriolis parameter; F_{Xn} and F_{Yn} are sources/sinks for the horizontal wind components that are archived in CRCM simulations, including surface friction, vertical diffusion, gravity wave drag. Lateral diffusion is an additional sink term that is not archived by CRCM; here we recompute its approximate contribution in the form of a ∇_h^4 diffusion applied on pressure surfaces, using the same constant as in the model: $c = 1.85 \times 10^{13} m^4 s^{-1}$ for the 45-km version of the CRCM (Laprise et al. 1998).

By using similar steps as described in the preceding section, the ensemble-mean and deviation equations of relative vorticity are written as:

$$\frac{\partial \langle \zeta \rangle}{\partial t} + \bar{\nabla} \cdot \langle \bar{V} \zeta \rangle + \left\langle \omega \frac{\partial \zeta}{\partial p} \right\rangle = -\bar{\nabla} \cdot \langle f \bar{V} \rangle + S \left[\left\langle \frac{\partial \omega}{\partial Y} \frac{\partial U}{\partial p} \right\rangle - \left\langle \frac{\partial \omega}{\partial X} \frac{\partial V}{\partial p} \right\rangle \right] + S \left[\frac{\partial \langle F_Y \rangle}{\partial X} - \frac{\partial \langle F_X \rangle}{\partial Y} \right] - c \nabla^4 \langle \zeta \rangle \quad (16)$$

and

$$\begin{aligned}
\frac{D\zeta'_n}{Dt} &\equiv \frac{\partial \zeta'_n}{\partial t} + \langle \bar{V} \rangle \cdot \bar{\nabla} \zeta'_n + \langle \omega \rangle \frac{\partial \zeta'_n}{\partial p} = -\zeta'_n \bar{\nabla} \cdot \langle \bar{V} \rangle - \bar{V}'_n \cdot \bar{\nabla} \langle \zeta' \rangle - \omega'_n \frac{\partial \langle \zeta' \rangle}{\partial p} - \langle \zeta' \rangle \bar{\nabla} \cdot \bar{V}'_n - \bar{\nabla} \cdot (\zeta'_n \bar{V}'_n) - \omega'_n \frac{\partial \zeta'_n}{\partial p} \\
&+ \bar{\nabla} \cdot (\zeta'_n \bar{V}'_n) + \left\langle \omega'_n \frac{\partial \zeta'_n}{\partial p} \right\rangle - \bar{\nabla} \cdot (f \bar{V}'_n) + S \left[\frac{\partial \langle \omega \rangle}{\partial Y} \frac{\partial U'_n}{\partial p} - \frac{\partial \langle \omega \rangle}{\partial X} \frac{\partial V'_n}{\partial p} \right] + S \left[\frac{\partial \omega'_n}{\partial Y} \frac{\partial \langle U \rangle}{\partial p} - \frac{\partial \omega'_n}{\partial X} \frac{\partial \langle V \rangle}{\partial p} \right] \quad (17) \\
&+ S \left[\frac{\partial \omega'_n}{\partial Y} \frac{\partial U'_n}{\partial p} - \frac{\partial \omega'_n}{\partial X} \frac{\partial V'_n}{\partial p} \right] + S \left[\left\langle \frac{\partial \omega'_n}{\partial X} \frac{\partial V'_n}{\partial p} \right\rangle - \left\langle \frac{\partial \omega'_n}{\partial Y} \frac{\partial U'_n}{\partial p} \right\rangle \right] + S \left[\frac{\partial F'_{Yn}}{\partial X} - \frac{\partial F'_{Xn}}{\partial Y} \right] - c \nabla^4 \zeta'_n
\end{aligned}$$

The inter-member variance equation for relative vorticity (σ_{ζ}^2) is obtained by

applying $\langle \zeta'_n \times (17) \rangle$, to get:

$$\begin{aligned}
\frac{1}{2} \frac{D\sigma_{\zeta}^2}{Dt} &\equiv \frac{\partial}{\partial t} \left(\frac{\sigma_{\zeta}^2}{2} \right) + \frac{\langle \bar{V} \rangle}{2} \cdot \bar{\nabla} \sigma_{\zeta}^2 + \frac{\langle \omega \rangle}{2} \frac{\partial \sigma_{\zeta}^2}{\partial p} = -\sigma_{\zeta}^2 \bar{\nabla} \cdot \langle \bar{V} \rangle - \langle \zeta'_n \bar{V}'_n \rangle \cdot \bar{\nabla} \langle \zeta' \rangle - \langle \zeta'_n \omega'_n \rangle \frac{\partial \langle \zeta' \rangle}{\partial p} - \langle \zeta' \rangle \langle \zeta'_n \bar{\nabla} \cdot \bar{V}'_n \rangle \\
&- \langle \zeta'_n \bar{\nabla} \cdot (f \bar{V}'_n) \rangle + S \left[\frac{\partial \langle \omega \rangle}{\partial Y} \left\langle \zeta'_n \frac{\partial U'_n}{\partial p} \right\rangle - \frac{\partial \langle \omega \rangle}{\partial X} \left\langle \zeta'_n \frac{\partial V'_n}{\partial p} \right\rangle \right] + S \left[\left\langle \zeta'_n \frac{\partial \omega'_n}{\partial Y} \right\rangle \frac{\partial \langle U \rangle}{\partial p} - \left\langle \zeta'_n \frac{\partial \omega'_n}{\partial X} \right\rangle \frac{\partial \langle V \rangle}{\partial p} \right] \\
&+ S \left[\left\langle \zeta'_n \frac{\partial F'_{Yn}}{\partial X} \right\rangle - \left\langle \zeta'_n \frac{\partial F'_{Xn}}{\partial Y} \right\rangle \right] - c \underbrace{\langle \zeta'_n \nabla^4 \zeta'_n \rangle}_{3^{rd} \text{ order}} - \underbrace{\langle \zeta'_n \bar{\nabla} \cdot (\zeta'_n \bar{V}'_n) \rangle - \left\langle \frac{\omega'_n}{2} \frac{\partial \zeta'^2_n}{\partial p} \right\rangle}_{3^{rd} \text{ order}} + S \left[\left\langle \zeta'_n \frac{\partial \omega'_n}{\partial Y} \frac{\partial U'_n}{\partial p} \right\rangle - \left\langle \zeta'_n \frac{\partial \omega'_n}{\partial X} \frac{\partial V'_n}{\partial p} \right\rangle \right] \quad (18)
\end{aligned}$$

where: $\sigma_{\zeta}^2 = \langle \zeta'^2 \rangle$

Furthermore, the variance equation for the absolute vorticity ($\sigma_{\eta}^2 = \langle (\eta'_n + f)^2 \rangle$)

can be derived using Eq. 18 (see *Appendix C* and *Appendix F*). The absolute and relative vorticity equations have similar terms because the first one differs from the second by the planetary vorticity.

When we use the continuity equation of the ensemble-mean flow (Eq. 9), the advection term of this last equation is rewritten into flux form as:

$$L_{\zeta} = R_{\zeta} = A_h + A_v + N_h + B_h + B_v + C + D + E_h + F_v + G + H \quad (19)$$

where,

$$\begin{aligned}
L_\zeta &= \frac{\partial \sigma_\zeta^2}{\partial t}; \\
A_h &= -\bar{\nabla} \cdot (\sigma_\zeta^2 \langle \bar{V} \rangle); & A_v &= -\frac{\partial (\sigma_\zeta^2 \langle \omega \rangle)}{\partial p}; & N_h &= -2\sigma_\zeta^2 \bar{\nabla} \cdot \langle \bar{V} \rangle \\
B_h &= -2 \left\langle \zeta'_n \bar{V}'_n \right\rangle \cdot \bar{\nabla} \langle \zeta \rangle; & B_v &= -2 \left\langle \zeta'_n \omega'_n \right\rangle \frac{\partial \langle \zeta \rangle}{\partial p} \\
C &= -2 \langle \zeta \rangle \left\langle \zeta'_n \bar{\nabla} \cdot \bar{V}'_n \right\rangle; & D &= -2 \left\langle \zeta'_n \bar{\nabla} \cdot (f \bar{V}'_n) \right\rangle; \\
E_h &= 2S \left[\frac{\partial \langle \omega \rangle}{\partial Y} \left\langle \zeta'_n \frac{\partial U'_n}{\partial p} \right\rangle - \frac{\partial \langle \omega \rangle}{\partial X} \left\langle \zeta'_n \frac{\partial V'_n}{\partial p} \right\rangle \right] \\
F_v &= 2S \left[\left\langle \zeta'_n \frac{\partial \omega'_n}{\partial Y} \right\rangle \frac{\partial \langle U \rangle}{\partial p} - \left\langle \zeta'_n \frac{\partial \omega'_n}{\partial X} \right\rangle \frac{\partial \langle V \rangle}{\partial p} \right]; \\
G &= 2S \left[\left\langle \zeta'_n \frac{\partial F'_{Yn}}{\partial X} \right\rangle - \left\langle \zeta'_n \frac{\partial F'_{Xn}}{\partial Y} \right\rangle \right] - 2c \left\langle \zeta'_n \nabla^4 \zeta'_n \right\rangle; \\
H &= -2 \left\langle \zeta'_n \bar{\nabla} \cdot (\zeta'_n \bar{V}'_n) \right\rangle - \left\langle \omega'_n \frac{\partial \zeta'^2}{\partial p} \right\rangle + 2S \left[\left\langle \zeta'_n \frac{\partial \omega'_n}{\partial Y} \frac{\partial U'_n}{\partial p} \right\rangle - \left\langle \zeta'_n \frac{\partial \omega'_n}{\partial X} \frac{\partial V'_n}{\partial p} \right\rangle \right]
\end{aligned}$$

The left-hand side term describes the local rate of change of the relative vorticity IV (term L_ζ), and the right-hand side, the nine contributions: A ($\equiv A_h + A_v$), N_h , B ($\equiv B_h + B_v$), C , D , E_h , F_v , G and H . Certain terms of this equation have physical representations analogous to those in Eq. 14. Notably, the term A relates to the IV transport by the ensemble-mean flow, the term B relates to the covariance of fluctuation (ζ'_n and \bar{V}'_n) in the direction of the gradient of the ensemble-mean relative vorticity ($\nabla \langle \zeta \rangle$). The term N_h is the divergence of the ensemble-mean horizontal wind acting upon IV. The term C couples the ensemble-means relative vorticity ($\langle \zeta \rangle$) and the covariance of perturbations of relative vorticity and horizontal divergence ($\langle \zeta'_n \bar{\nabla} \cdot \bar{V}'_n \rangle$). Coriolis effects are taken into account through the term D that represents a covariance. Terms E_h and F_v are issued from the tilting-twisting term of the vorticity equation. The term G is the sum of two covariance terms involving perturbation relative vorticity: the first is a coupling with the horizontal gradient of

sources/sinks of momentum, and the last one is associated with the lateral diffusion. The last term (H) regroups third-order terms.

2.3. Domain, Simulation and Evaluation methods

This present study uses archived CRCM simulations described by Alexandru et al. (2007). The study domain covers the east of the North American domain and a part of Atlantic Ocean (see Fig. 1 in Alexandru et al. (2007) for CRCM computational domain). The CRCM (version 3.6.1) grid is projected on polar stereographic coordinates with a 45-km grid mesh (true at 60° latitude). The archive corresponds to 20-member simulations carried on computational domain of 120 x 120 grid points in the horizontal. The model uses 18 Gal-Chen levels in the vertical and 15-min timestep. The simulated fields were interpolated on the following set of pre-specified pressure levels: 10, 20, 30, 50, 70, 100, 150, 200, 250, 300, 400, 500, 600, 700, 850, 925, 1000 and 1050 hPa. The 1050-hPa level is an extrapolation of the 1000-hPa level. The archived fields are available at 6-hourly intervals; atmospheric variables correspond to samples at archival time, whereas the source/sink terms correspond to cumulative contributions between archival times.

The budget equations for inter-member variance of potential temperature and relative vorticity (Eq. 14 and Eq. 19), respectively, will be used to diagnose the various contributions to the time evolution of the IV. All terms of these equations are evaluated using the ensemble of 20-members simulations with CRCM. All the simulations use the same LBC for atmospheric fields, the same prescribed sea surface temperature (SST) and sea ice coverage, but differ only in their initialisation time. Each integration starts successively with data from the first twenty days (valid at 0000 UTC) of May 1993; so that the only difference between two successive members is the delay of 24 hours at the beginning of each run. All simulations were run for three months of the 1993 summer and data were archived each 6 hours from 0000 UTC 1 June to 0000 UTC 1 September of 1993. So, we have a total of $\tau=369$ archives for these three months.

To perform the budget study of the IV, all terms of the left-hand (L_φ) and the right-hand (R_φ) sides will be assessed using standard discretisation methods. The inter-member variance tendency in Eq. 14 and Eq. 19 is calculated as second-order finite differences using leap-frog scheme as:

$$L_\varphi(i, j, k, t) \approx \frac{\sigma_\varphi^2(i, j, k, t + \Delta t) - \sigma_\varphi^2(i, j, k, t - \Delta t)}{2\Delta t} \quad (20)$$

where φ represents either potential temperature (θ) or relative vorticity (ζ), and $\Delta t = 6h$.

The right-hand (R_φ) side is the sum of several terms, depending of the equation. For the potential temperature, it is evaluated using discretisation as follows:

$$R_\theta(i, j, k, t) = [A_h + A_v + B_h + B_v + C + E_h + E_v](i, j, k, t) \quad (21)$$

with

$$\begin{aligned} A_h &\approx -S \left[\delta_x \left(\overline{U}^x \overline{\sigma_\theta^2}^x \right) + \delta_y \left(\overline{V}^y \overline{\sigma_\theta^2}^y \right) \right]; \quad A_v \approx -\delta_p (\langle \omega \rangle \sigma_\theta^2) \\ B_h &\approx -2S \left[\langle \theta'_n U'_n \rangle \delta_x \overline{\langle \theta \rangle}^x + \langle \theta'_n V'_n \rangle \delta_y \overline{\langle \theta \rangle}^y \right]; \quad B_v \approx -2 \langle \theta'_n \omega'_n \rangle \delta_p \langle \theta \rangle \\ C &\approx 2 \langle \theta'_n Q'_n \rangle - 2c \langle \theta'_n \nabla^4 \theta'_n \rangle \quad \text{where } Q'_n = \frac{1}{c_p} \left(\frac{p_0}{p} \right)^\kappa (Q'_p + Q'_{dv} + Q'_c + Q'_r)_n \\ E_h &\approx -2S \left[\left\langle \theta'_n \delta_x \left(\overline{\theta'}^x \overline{U'_n}^x \right) \right\rangle + \left\langle \theta'_n \delta_y \left(\overline{\theta'}^y \overline{V'_n}^y \right) \right\rangle \right]; \quad E_v \approx -2 \langle \theta'_n \delta_p (\omega'_n \theta'_n) \rangle \end{aligned} \quad (22)$$

where the first-order difference and average operators ($\delta_x, \delta_y, \delta_p, \overline{(\)}^x, \overline{(\)}^y$) are defined in the *Appendix C*. Q'_p, Q'_{dv}, Q'_c and Q'_r represent, respectively, the ensemble mean deviation of heating by condensation (latent heating), vertical

diffusion, convection, and radiation. The pressure-coordinate vertical motion ($\omega \equiv dp/dt$) is not directly archived as CRCM output data, so it is approximated using the geopotential height (ϕ) and vertical velocity ($w \equiv dz/dt$) data; the details of this computation are given in *Appendix E*.

For the relative vorticity, the right-hand side is calculated using this following notation:

$$R_\zeta(i, j, k, t) = [A_h + A_v + N_h + B_h + B_v + C + D + E_h + F_v + G + H](i, j, k, t) \quad (23)$$

where the evaluation of different symbols are given in *Appendix D*.

We will regularly use space and/or time average to reduce the dimensionality of the fields in our analysis:

- Spatial average of a variable $\varphi(i, j, k, t)$:

$$\bar{\varphi}^{xy}(k, t) = \frac{1}{I \times J} \sum_{i=1}^I \sum_{j=1}^J \varphi(i, j, k, t) \quad (24)$$

where I and J designate the number of grid intervals in x and y direction of the diagnostic domain of interest.

- Time average of $\varphi(i, j, k, t)$:

$$\bar{\varphi}'(i, j, k) = \frac{1}{\tau} \sum_{t=1}^{\tau} \varphi(i, j, k, t) \quad (25)$$

where τ represents the number of archived fields in the period of interest.

3. Results and Analysis

3.1. Vertical profile and time evolution of the IV

Before proceeding to apply the diagnostic budget equations for IV that we have developed, we will begin by reviewing some characteristics of IV that developed in the 20-member ensemble simulations of Alexandru et al. (2007). We will look first at

the vertical profile of time- and domain-averaged IV. We will then look at the time evolution of domain-mean IV at selected vertical levels. We will then show maps of IV on selected pressure levels. Finally we will present maps of time-averaged IV (Eq. 25) at different times and pressure levels. Figures 1a and 1d show vertical profiles of the time- and domain-averaged IV for potential temperature and relative vorticity, respectively, computed using Eq. 5, and then time-averaged over the 3-month period (Eq. 25) and space-averaged over the sub-domain (Eq. 24) indicated in Fig. 2a; this selected domain contains 100×70 grid points and excludes the 10-grid point sponge zone and a spatial spin-up area of a few grid points along the western lateral boundary. The two atmospheric variables exhibit similar vertical profiles of IV, with a maximum near the ground, a minimum around 600-700 hPa, and another maximum near the tropopause (200-300 hPa). We note that the amplitude of the time- and space-average IV is rather modest compared to transient-eddy variability: standard deviation of IV is a few tenth of a degree for potential temperature and of order of 10^{-5} s^{-1} for relative vorticity. In the following analysis, we will concentrate on three standard levels where IV is either a maximum or a minimum, on average, for each variable.

Figures 1b and 1e show the time evolution IV of potential temperature and relative vorticity, respectively, in the 20-member simulations. These figures reveal that the IV fluctuates greatly in time, with long periods of relatively weak IV and occasional episodes of intense IV at certain times. A particularly intense episode occurred between 16 and 28 July 1993, with the most intense IV occurring near the surface and close to the tropopause, and smaller values in mid-troposphere (Fig. 1c and 1f focus on this period). For the potential temperature at 200 hPa, we note a rapid increase of IV, from $\sim 0.10 \text{ K}^2$ on July 18 to $\sim 1.02 \text{ K}^2$ July 20, and an equally rapid decrease from July 20 to July 22 July (Fig. 1c). At 300 hPa, the IV follows a similar trend pattern as that at level 200 hPa (result not shown). A growth of IV also takes place at 925 hPa, but the maximum is reached a day and a half later, on July 21 at 12Z, and the maximum is weaker (of $\sim 0.35 \text{ K}^2$). At 700 hPa level, the variations are

quite modest. During roughly the same period, the maximum IV in relative vorticity occurs at low levels (Fig. 1f), with values growing from $\sim 1.3 \times 10^{-10} \text{ s}^{-2}$ on July 16 to $\sim 5.2 \times 10^{-10} \text{ s}^{-2}$ on July 20, and a rapid decrease after July 24. Alexandru et al. (2007) have also noted large variations of the IV in this period for the 850-hPa geopotential. The 300-hPa IV follows a similar trend pattern, but with somewhat weaker amplitude. Again IV amplitudes are weakest in the mid-troposphere.

Figure 2 presents maps of the time-averaged potential temperature and relative vorticity IV at three selected levels. At upper level, we note rather similar spatial distribution of the IV for both studied variables; the maximum of IV seems to be spread from the south-eastern United States towards the northeast part of the domain where the largest intensities are achieved, which corresponds to the upper air outflow region, as was noted by Lucas-Picher et al. (2008). Right at the boundary, the RCM solution is forced back to the driving flow, so the IV decreases to zero because, by design, all members share the same LBC. The relative vorticity IV show intense values over a small area over Alabama at all levels, as noted by Alexandru et al. (2007) who studied the distribution of precipitation and geopotential IV. They found that the IV centre is initially formed over the southern US (Georgia, South Carolina, Alabama), then, in the following days, it intensifies and moves north-eastward along the storm track. We note that the IV of relative vorticity is very intense over a broad region at low level, whereas the maximum IV in potential temperature is mostly concentrated in the north-east corner of the domain and at upper level.

In Figure 3 and 4, we present maps of the IV at two levels where maximum amplitude occurs and at selected times during the period of rapid increase (from 17 to 21 July). The various panels allow tracking the trajectory of the maximum IV. We commented earlier on the rapid large decreases of the IV for both of the studied parameters after 20 July; as it can be seen in Figure 3 and 4, the large decrease of IV occurs when the maximum IV is close to the northeast boundary and eventually exits the domain.

For the rest of this study, the period of large changes in IV (16-28 July) will be used to analyze the different contributions to the variations in IV.

3.2. Validation of the Internal Variability budget equation

We now turn to the diagnostics equations we developed earlier to explain the tendency of IV (Eq. 14 and Eq. 19) for the potential temperature and for the relative vorticity, respectively. As a first step, we will compare the left-hand side term ($L_\varphi(i, j, k, t)$), i.e. the tendency of IV in the 20-member ensemble of Alexandru et al. (2007) computed with (20), with the sum of all the right-hand side terms ($R_\varphi(i, j, k, t)$) computed from the detailed expressions in (21) and (23) using the archived samples of the simulated fields. We do not expect to reproduce the model's simulated behaviour perfectly given the numerous approximations made in evaluating the right-hand side terms, such as interpolations from model terrain-following coordinate to selected pressure levels, six-hourly sampling, advection with second-order Eulerian finite differences rather than semi-Lagrangian transport in CRCM, and approximations to calculate ω , but we hope at least for qualitative or some semi-quantitative correspondence between the left- and right-hand side terms.

3.3. Spatial patterns of the internal variability tendency

Figure 5 presents the fields of the left-hand side term ($L_\vartheta(i, j, k, t)$) and the right-hand side term ($R_\vartheta(i, j, k, t)$) of the IV tendency equation for potential temperature (Eq. 14) at two pressure levels, each day from 18 to 21 July. We note good qualitative agreement between these two terms. To illustrate the correspondence between them and to get a more quantitative evaluation, we present dispersion diagrams in Figure 7A using all grid points of the study domain (except the sponge zone) for July 19 and 20, and we compute correlation coefficients. At the 200-hPa level, the correlation coefficients on 19 and 20 July at 0000 UTC are 0.80 and 0.84,

respectively. On these same dates, the correlation coefficients at the 925-hPa level are 0.77 and 0.87, respectively (see Fig. 7A).

Figure 6 presents the corresponding fields of the left- and the right-hand side terms of the IV tendency equation for relative vorticity (Eq. 19) at two pressure levels, each day from 18 to 21 July. Because relative vorticity is a noisier field than potential temperature, so is the IV tendency. Nevertheless the results also show a good qualitative agreement between the left- and right-hand side terms. Figure 7B shows the corresponding dispersion diagrams and correlation coefficients. On 19 July 1993, the correlation coefficients between these two terms are 0.90 and 0.84 at 300- and 925-hPa levels, respectively; and on 20 July 1993, correlations are 0.88 and 0.84 at these same pressure levels, respectively.

3.4. Time evolution of the domain-average internal variability tendency

Next we compare in Figure 8 the time evolution of the left- and the right-hand side terms during the period of interest, averaged over the selected domain (see Fig. 2a). The time evolutions denote fairly good agreement, with correlations coefficient of 0.96 at 200 and 925 hPa for potential temperature, and 0.85 and 0.91 at 300 and 925 hPa, respectively, for relative vorticity. The diagnostics hence appears to provide a fairly robust correspondence between the two components, L_ϕ of the IV that developed in the 20-member ensemble and R_ϕ that evaluates diagnostically the contributions to the IV using the archived data. So, we now proceed to analyse the different contributions to the right-hand side term in order to gain some understanding of the physical mechanisms responsible for the development and evolution of IV in regional model simulations.

The previous results suggest that the developed tendency equations can be used to understand the physical processes that lead to large IV in certain periods in the simulation ensemble of Alexandru et al. (2007). In other words, the $R_\phi(i, j, k, \iota)$

terms can be diagnosed to identify the contribution of each term to the increase of the IV. The next sections will be devoted to this study.

3.4.1. Budget of the potential temperature IV

We now proceed to study the various contributions to the time evolution of potential temperature IV as presented in Eq. 22. Figure 9a shows the vertical profiles of the left- and right-hand side terms of the potential temperature IV equation for the 18 and 19 July 1993 at 0000 UTC, averaged over the analysis domain. During this period, a rapid increase of IV tendency occurred near the tropopause level, with two maxima at 200- and 300-hPa levels. Figures 9b and 9c show the vertical profile of the contributions to the right-hand side term. On July 18, when the IV was rather small and almost constant in the vertical, Figure 9b shows that in fact two terms were quite large but opposing one another: the C term contributed to IV growth throughout the troposphere while the B_v term contributed equally but with the opposite sign, resulting in very small net tendency. On July 19, the IV was growing rapidly at 200- and 300-hPa levels; Figure 9c shows very large contributions from the C and B_v terms (note the different scale), mostly compensating one another below the 250-hPa level. At 200 hPa, the term B_v is mainly responsible for the net tendency, while at 300 hPa the larger positive C term dominates over the negative B_v term. Figures 9b and 9c show that large contributions of terms B_v and C are noted at 400- and 850-hPa pressure levels.

Figures 10a and 10b show the time evolution of IV tendency during the period of interest at 200 and 925 hPa levels. At 200 hPa, B_v tends to be positive while C is generally negative, except during a brief period around July 19-20 when it is positive (Fig. 10a). The term A_h is occasionally important, contributing negatively to IV tendency. At 925 hPa where the potential temperature IV tendency is somewhat weaker, Figure 10b shows that B_h and C are mainly positive and B_v is mainly negative (see also Fig. 11B), hence partly compensating one another. This last result is noted

throughout the troposphere (between 250 hPa and 1000 hPa – see Fig. 9b and Fig. 9c).

The analysis of term C reveals that condensation (C_{cond}) and convection (C_{conv}) are the two main processes that are responsible for its large positive contribution in the troposphere (Fig. 13e,f). Radiation (C_{rad}) contributes little, while horizontal and vertical diffusion (C_{Dh} and C_{Dv} respectively) contributes negatively to the tendency, as is to be expected (see Fig. 13e,f). Therefore, the IV growth results primarily from covariances of fluctuations of potential temperature with diabatic heating from condensation and convection, which act to heat the regions of warm perturbations.

The potential temperature IV growth is greatly reduced by the negative contribution from B_v , which is made of two terms: the covariance of fluctuations of potential temperature with vertical motion ($\langle \theta'_n \omega'_n \rangle$) and the ensemble-mean vertical gradient of the potential temperature ($\partial \langle \theta \rangle / \partial p$). The latter factor is always negative due to the stable stratification of the ensemble-mean atmosphere (see Fig. 13b). The covariance $\langle \theta'_n \omega'_n \rangle$ is negative with large amplitude during episodes of large growth of IV (see Fig. 13a), as was noted from 18 to 28 July (Fig. 1c). Physically, a negative covariance means that warm air ($\theta'_n > 0$) rises ($\omega'_n < 0$) and cold air ($\theta'_n < 0$) sinks ($\omega'_n > 0$) on average, in perturbations from ensemble-mean conditions. A negative covariance $\langle \theta'_n \omega'_n \rangle$ hence implies a decay of potential temperature IV, which is equivalent to a baroclinic conversion from perturbation potential energy to perturbation kinetic energy (e.g. Lorenz 1955, 1967).

So to summarise: during the episode under study, the large growth of potential temperature IV results from covariance of potential temperature with diabatic heating from condensation and convection (by heating the warm perturbations), while the covariance of vertical motion and potential temperature (rising warm and sinking cold perturbations) contributes to reduce the IV growth through baroclinic conversion of perturbation potential energy to perturbation kinetic energy.

We have also analysed the term B_h , which contributes slightly to the IV growth (see Fig. 9b, 9c and 10b). The positive contribution of B_h implies that, on average, the vector of the covariance of fluctuations ($\langle \theta'_n \bar{V}'_n \rangle$) is in the opposite sign to the horizontal gradient vector ($\bar{\nabla} \langle \theta \rangle$) throughout the troposphere. Results show that, during this episode, $\langle U'_n \theta'_n \rangle < 0$ and $\langle V'_n \theta'_n \rangle > 0$ (see Fig. 14A), and the mean potential temperature increases south-eastward ($\partial \langle \theta \rangle / \partial X > 0$, $\partial \langle \theta \rangle / \partial Y < 0$). Physically, this implies transport of cold perturbations ($\theta'_n < 0$) eastward ($U'_n > 0$) and/or warm perturbations northward, hence heat transport by perturbations “down the gradient” of ensemble-mean potential temperature, which favours the growth of IV during this episode. This is the equivalent, in the context of perturbations from an ensemble mean, to a baroclinic conversion of available potential energy from the mean state to the perturbations component.

On average during the episode under study, the horizontal transport term (A_h) has small magnitude and does not contribute substantially to the variation of the IV when integrated over the whole domain; this term corresponds to the horizontal displacement of the IV with the mean flow. The A_h contributes occasionally to decrease IV when regions of large IV are moving out of the regional domain.

The third-order terms (E_h and E_v) have very small magnitude when integrated over the domain (Fig. 10a,-b); the term E_h can locally contribute to variations of the IV (see Fig. 11), contrary to E_v which remains very weak even when the IV is large.

3.4.2. Budget of the relative vorticity IV

As with potential temperature IV, we now proceed to evaluate the contribution of each term on the right-hand side of the relative vorticity IV equation (Eq. 19).

Figure 9d shows vertical profiles of the domain average of L_ζ and R_ζ of the relative vorticity IV equation on July 18 and 19, 1993. We note an increase of the IV

tendency at all levels during this period. Figures 9e and 9f present the vertical profiles of the domain average of all terms of R_ζ (Eq. 23) on these two days. G is generally negative at all levels during the period of interest (see Fig. 10c,-d). Contrary to potential temperature IV, the covariance term B_v involving vertical motion perturbations has a weak magnitude (Fig. 9e,-f and Fig. 10c,-d), and the covariance term B_h involving horizontal wind perturbations acts as a production term for the relative vorticity IV. The results show that, on average, the covariance of fluctuation of horizontal winds with relative vorticity $\langle \zeta'_n \bar{V}'_n \rangle$ has a positive sign for both components (see Fig. 14B), while the ensemble-mean state has gradients $\partial\langle\zeta\rangle/\partial X < 0$ and $\partial\langle\zeta\rangle/\partial Y < 0$, indicating transport of perturbation cyclonic vorticity down-the-gradient of the ensemble-mean relative vorticity, resulting in production of relative vorticity IV at the expense of ensemble-mean state.

The time evolution of all right-hand side terms at 300 and 925 hPa shows that, on average, terms C and D have positive sign, in particular at low levels (see Fig. 10e and 10f). Figure 12 shows the spatial pattern of each term on the right-hand side of the relative vorticity IV equation on July 20 1993 at 300 and 925 hPa. Both terms involve covariance of perturbations of horizontal wind divergence and relative vorticity. A positive contribution of the term C implies that cyclonic (anticyclonic) perturbations are associated with convergence (divergence), when the ensemble-mean state is cyclonic; this makes sense particularly in the planetary boundary layer due to Ekman pumping with surface friction. Similarly, a positive contribution of the term D implies that cyclonic (anticyclonic) perturbations are associated with convergence (divergence), given that the Coriolis parameter varies slowly on the scale of weather perturbations.

We note that the terms E_h and F_v have weak contributions to IV variations (see Fig. 12). On average, the third-order terms (H) are negligible (see Fig. 9e and 9f and Fig. 10c and 10d); however, this term becomes large when the IV is large, as it can be seen in Figures 12 on 20 July when the IV reaches its maximum value.

Results reveal that the term G involving diffusion is negative, as ought to be expected, and it tends to reduce the positive contributions from production terms to the growth of IV (see Fig. 9e and 9f and Fig. 10c and 10d). The main production terms for relative vorticity IV are B_h , C and D . The transport term A acts to decrease IV by transporting high IV value out of the regional domain. Similarly the term N_h increases (decreases) the IV through convergence (divergence) by the ensemble-mean motion.

4. Conclusions

The purpose of this study was to understand the physical processes responsible for the development and fluctuations of internal variability (IV) in simulations of a nested regional climate model. Here IV is defined as the inter-member variance in an ensemble of simulations that differ only in their initiation time. This was addressed by performing a quantitative diagnostic calculation of the various diabatic and dynamical contributions to the time variation and spatial distribution of IV in the fields of potential temperature and the relative vorticity. The equations for potential temperature and the relative vorticity IV present similar terms, notably terms relating to the transport of IV by ensemble-mean flow and to the covariance of fluctuations acting on the gradient of the ensemble-mean state.

We studied an ensemble of 20-member simulations that differ only in their initial conditions (IC), as produced and described by Alexandru et al. (2007). We analyzed the contributions of the various dynamical and diabatic terms to the development and evolution of IV. We focused our analysis on a period and an area of interest characterized by a large IV. The various terms in the equations for the time tendency of IV were calculated diagnostically on pressure coordinates from the archived data of an ensemble of model simulations. In so doing, several interpolations and discretisation approximations were necessary in order to be able to compute the complex terms in the IV equations. Despite these approximations, the results showed good qualitative agreement, and sometimes even reasonable quantitative agreement,

for the time evolution and spatial distribution of IV, between our diagnostic computations (the so-called right-hand side) and the IV in the ensemble of simulations (the so-called left-hand side), with correlation coefficients above 0.75 and as high as 0.90 at some pressure levels. These encouraging results provide hope that the different contributions to the IV equation can be identified with our diagnostic budget approach.

Results show that IV maxima are found in the lower (925-1000 hPa) and upper (200-300 hPa) of the troposphere, with minima around 600-700 hPa. The large variations of the IV are noted from 16 to 28 July 1993 associated with strong synoptic events in the simulation, as was mentioned by Alexandru et al. (2007). Results reveal that the dominant terms responsible for the large increase of IV are either the covariance term involving the potential temperature fluctuations and diabatic heating fluctuations, or the covariance of inter-member fluctuations acting upon ensemble-mean gradients. Results also reveal that the episodes of large decreases of IV occur when the maxima of IV are close to the northeast boundary, and eventually get transported out of the regional domain by the ensemble-mean flow.

The dominant terms to the potential temperature IV tendency are:

$$B_h = -2 \langle \theta'_n \bar{V}'_n \rangle \cdot \bar{\nabla} \langle \theta \rangle, \quad B_v = -2 \langle \theta'_n \omega'_n \rangle \frac{\partial \langle \theta \rangle}{\partial p} \quad \text{and} \quad C = 2 \langle \theta'_n J'_n \rangle$$

The term C has the most important contribution to the IV growth, in particular due to the convection and condensation contributions to J'_n . The term B_v has similar magnitude as C throughout the troposphere, but with opposite sign: B_v contributes to decreasing IV because the gradient of the ensemble-mean potential temperature $\partial \langle \theta \rangle / \partial p$ is negative, reflecting that the ensemble-mean state of the atmosphere is statically stable, and the covariance of fluctuations in potential temperature and vertical motion $\langle \theta'_n \omega'_n \rangle$ is also negative, corresponding to warm fluctuations rising and cold fluctuations subsiding. Hence fluctuation available potential energy is generated by condensation and convection processes (term C), and this energy is

converted back to fluctuation kinetic energy. The B_h term has a weak positive contribution to the potential temperature IV tendency: the transport of heat by covariance of fluctuations of potential temperature and horizontal winds is down-the-gradient in the ensemble-mean state. This corresponds to a conversion from ensemble-mean available potential energy towards fluctuations available potential energy, contributing to the growth of the potential temperature IV.

The dominant terms to the relative vorticity IV tendency are:

$$B_h = -2 \langle \zeta'_n \bar{V}'_n \rangle \cdot \bar{\nabla}_h \langle \zeta \rangle, \quad C = -2 \langle \zeta \rangle \langle \zeta'_n \bar{\nabla} \cdot \bar{V}'_n \rangle, \quad D = -2 \langle \zeta'_n \bar{\nabla} \cdot (f \bar{V}'_n) \rangle$$

$$\text{and} \quad G = 2 \left[S \left(\left\langle \zeta'_n \left(\frac{\partial F'_{y_n}}{\partial X} - \frac{\partial F'_{x_n}}{\partial Y} \right) \right\rangle \right) - c \langle \zeta'_n \nabla^4 \zeta'_n \rangle \right]$$

Unlike the case for potential temperature, we note that all the terms are associated with horizontal components, suggesting that the IV of the relative vorticity is associated with the horizontal flow, which makes sense given the essentially geostrophic balance flow at the scale of the simulations. The term B_h contributes to the growth of relative vorticity IV: the transport of relative vorticity by covariance of fluctuations of relative vorticity and horizontal winds is down the gradient in the ensemble-mean state during episodes of large growth of relative vorticity IV. The terms C and D have also a positive contribution to the IV tendency during episodes of large growth, particularly at low levels; this implies that fluctuations with cyclonic (anticyclonic) circulation are associated with fluctuations with convergence (divergence) flow. We noted that episodes of large IV growth usually occur where and when the ensemble-mean state is cyclonic. All the positive contributions to the IV tendency are damped by the dissipation term G resulting mainly from the horizontal diffusion ($-2c \langle \zeta'_n \nabla^4 \zeta'_n \rangle$).

For potential temperature as well as for relative vorticity, the horizontal transport terms A_h by the ensemble-mean flow do not contribute much to the IV tendency, except to advect large IV pockets out of the regional domain, which then

explains the episodes of rapid decrease of IV. On average, the third-order terms have a weak contribution but they can be important when the IV is large.

The budget diagnostics of IV in this study has shed some light on the physical processes responsible for the development of IV and its fluctuations in time. This study however was limited to only one climate regime, for a domain located in mid-latitudes, on the East Coast of North America, for one season of one year, summer 1993, for a regional domain comprising 120 by 120 grid points, with one resolution using a grid mesh of 45 km, and the simulations were performed with one nested regional model, the CRCM. It is well documented that IV can greatly vary with weather regime, season, and domain size; similar studies should also be done for different configurations and climate regimes to ascertain which of the present conclusions are general and which are specific to the present configuration.

Acknowledgements This research was done as the Masters project of the first author, as a project within the Canadian Regional Climate Modelling and Diagnostic (CRCMD) Network, which is financially supported by the Canadian Foundation for Climate and Atmospheric Science (CFCAS) and the Ouranos Consortium. Ouranos also provided local facilities. The authors are indebted to Dr. G. J. Boer (CCCma) for suggesting the diagnostic methodology. We would like to thank to Mourad Labassi and Abderrahim Khaled for maintaining user-friendly local computing facility, and to Mrs Adelina Alexandru for allowing us to use her simulated data.

FIGURES

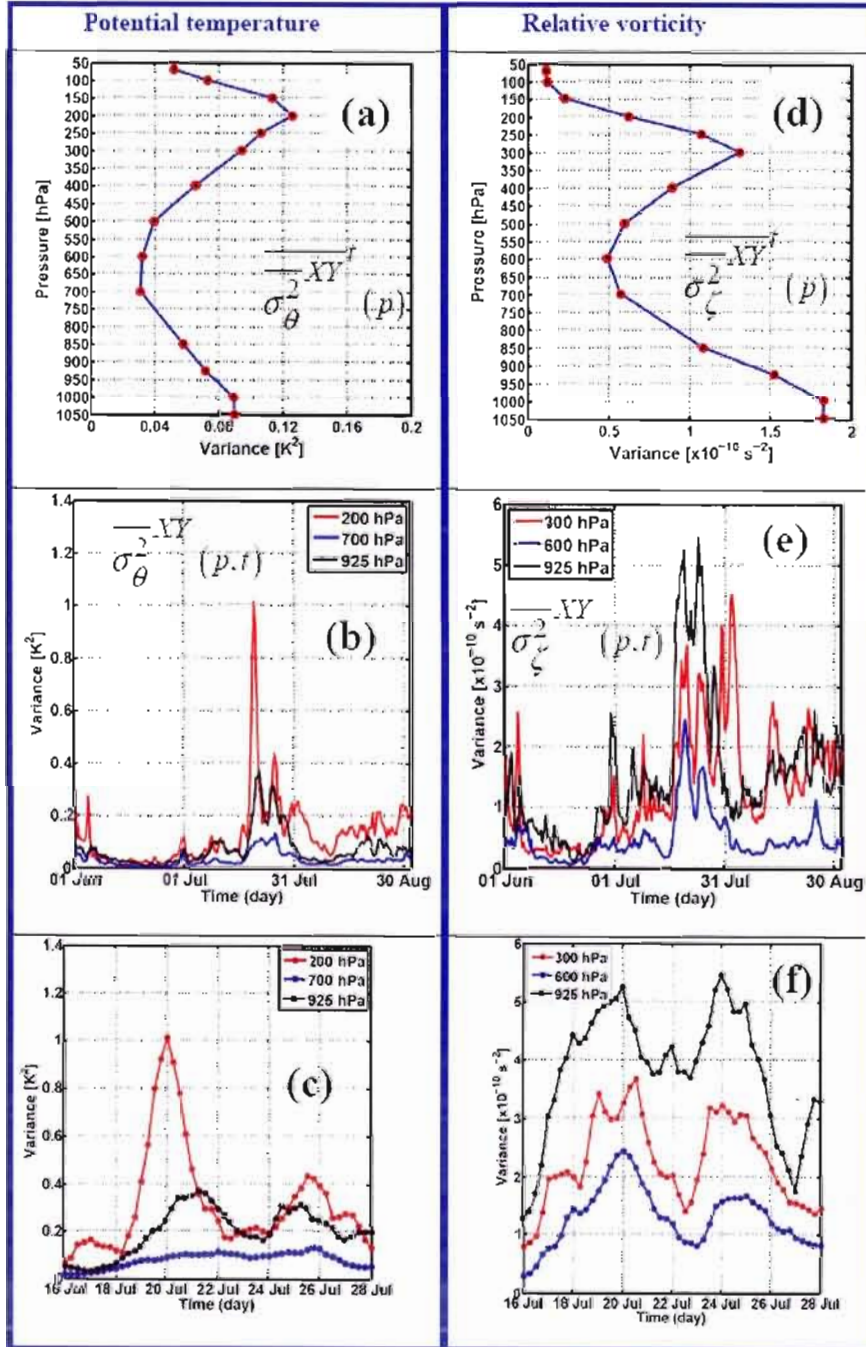


Figure 1: (a, d) Vertical profile of time- and domain-averaged inter-member variance for the potential temperature and the relative vorticity. The 1050-hPa level is an extrapolation of the 1000-hPa level; (b, c, e, f) Time evolution of the domain average variance for the potential temperature and relative vorticity at different pressure levels.

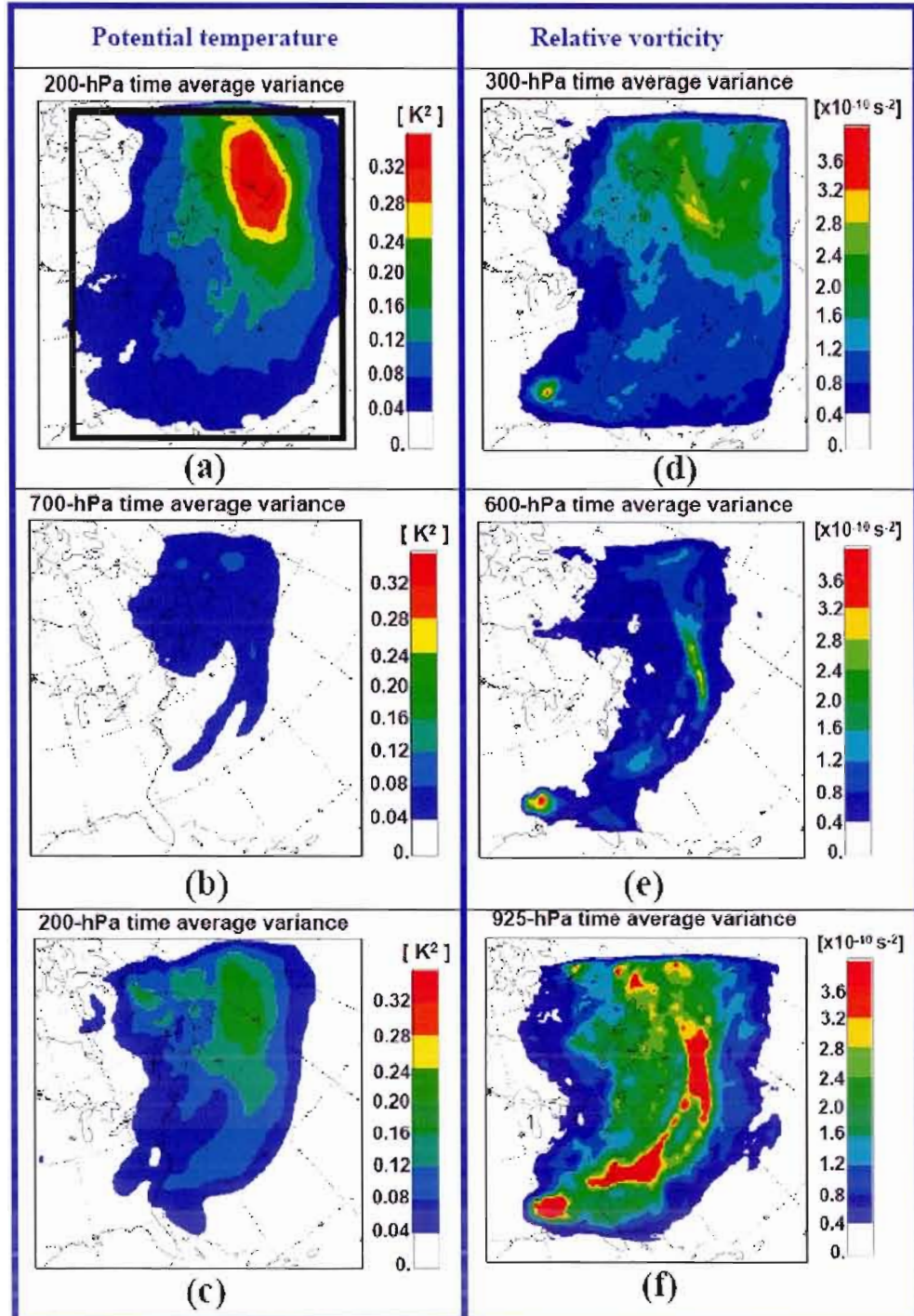


Figure 2 : Time-averaged over 3-month period of the inter-member variance for the potential temperature (a, b, c) and the relative vorticity (d, e, f). The domain of interest is shown in Figure 2a.

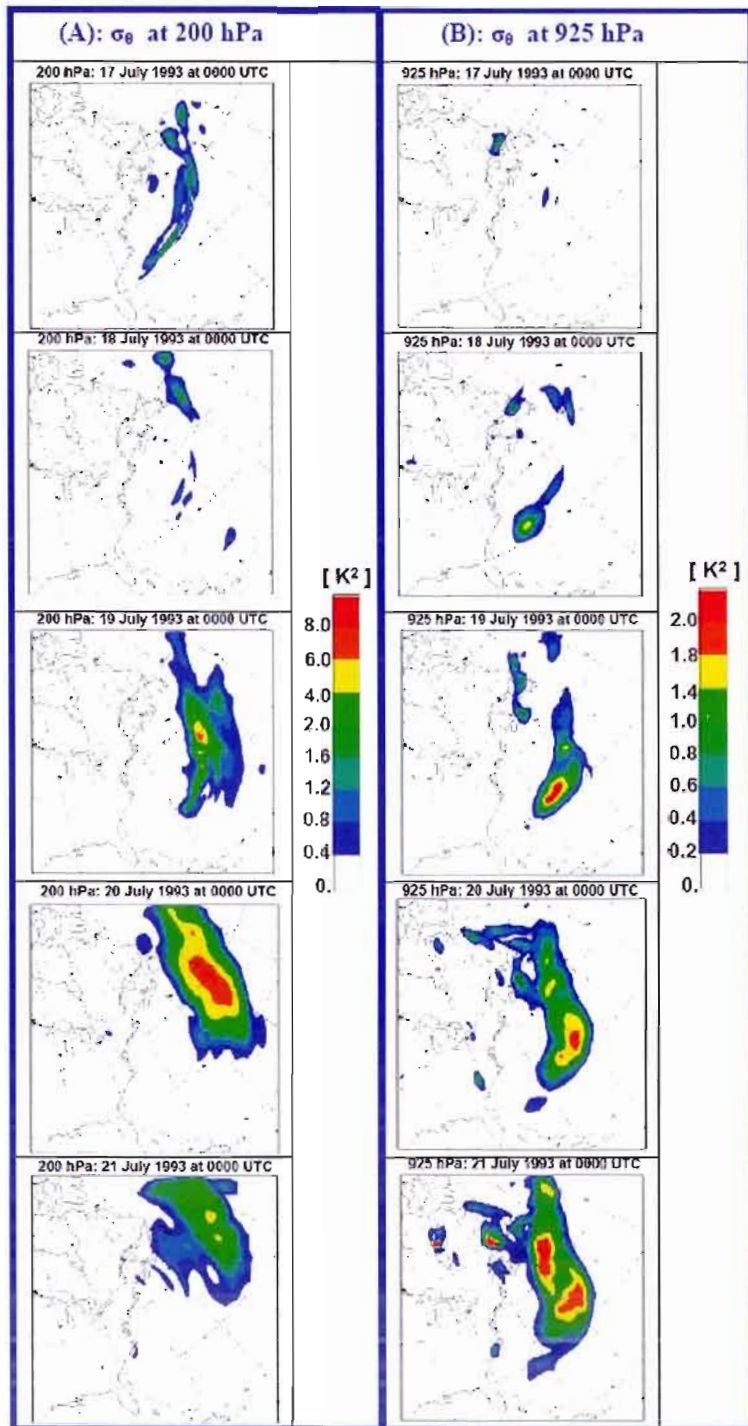


Figure 3: Field of inter-member variance for the potential temperature at (A) 200 hPa and (B) 925 hPa, during the period of large increase of IV from 17 to 21 July (see Figure 1c).

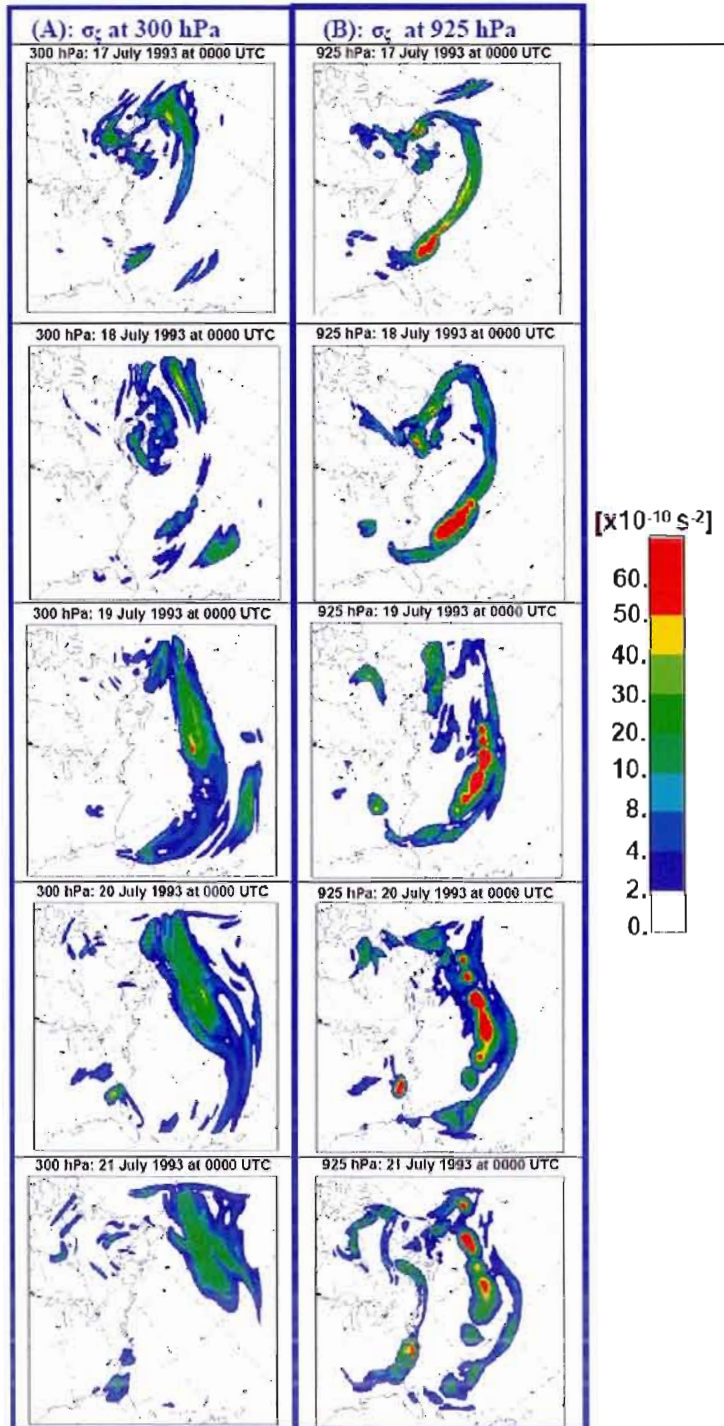


Figure 4: Field of inter-member variance for the relative vorticity at (A) 300 hPa and (B) 925 hPa, during the period of the large increase of IV from 17 to 21 July (see Fig. 1f).

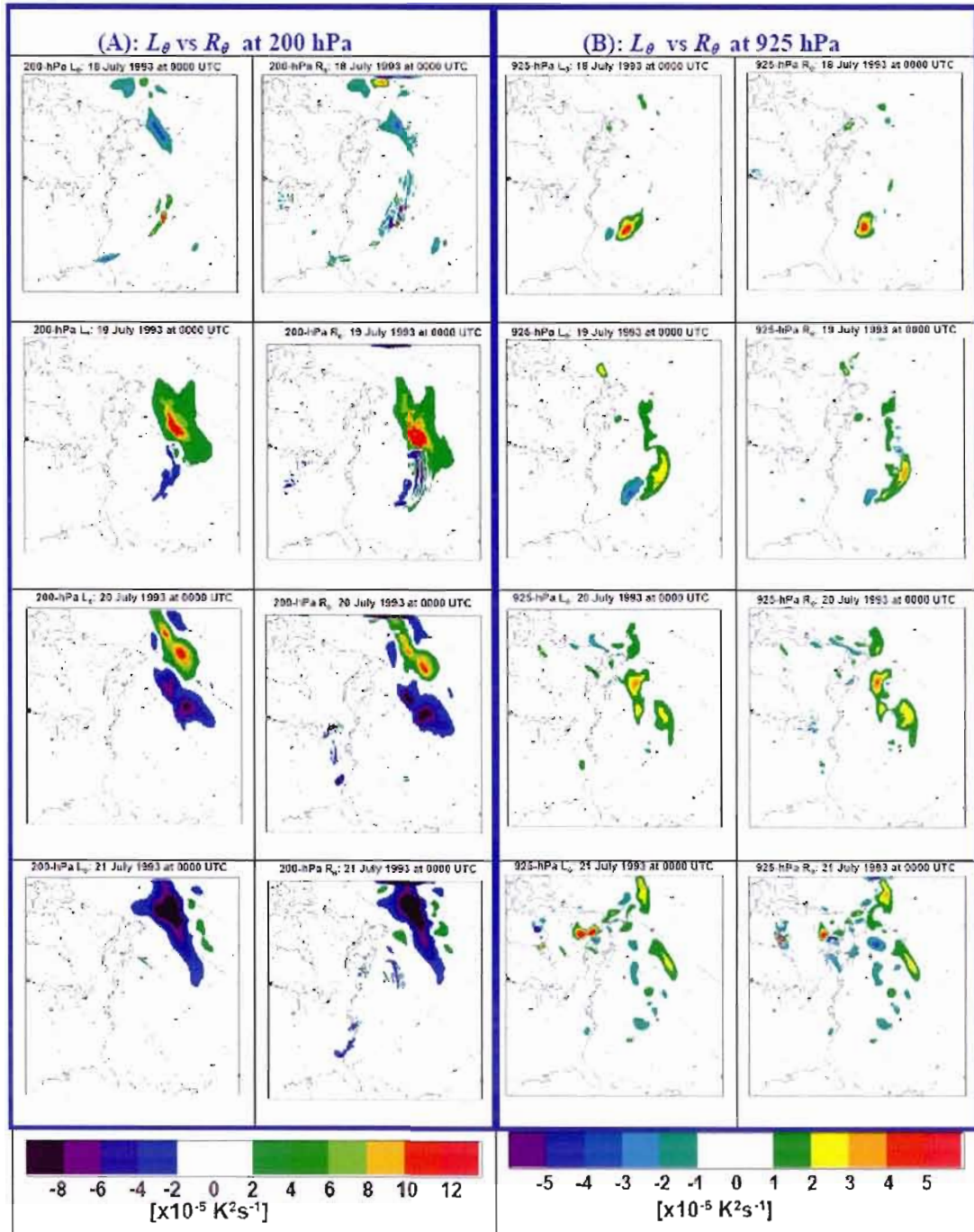


Figure 5 : Left-hand side term (L_θ) and the sum of all right-hand side term (R_θ) of the potential temperature inter-member variance equation on certain dates of the period of interest at different pressure levels: (A) 200 hPa and (B) 925 hPa.

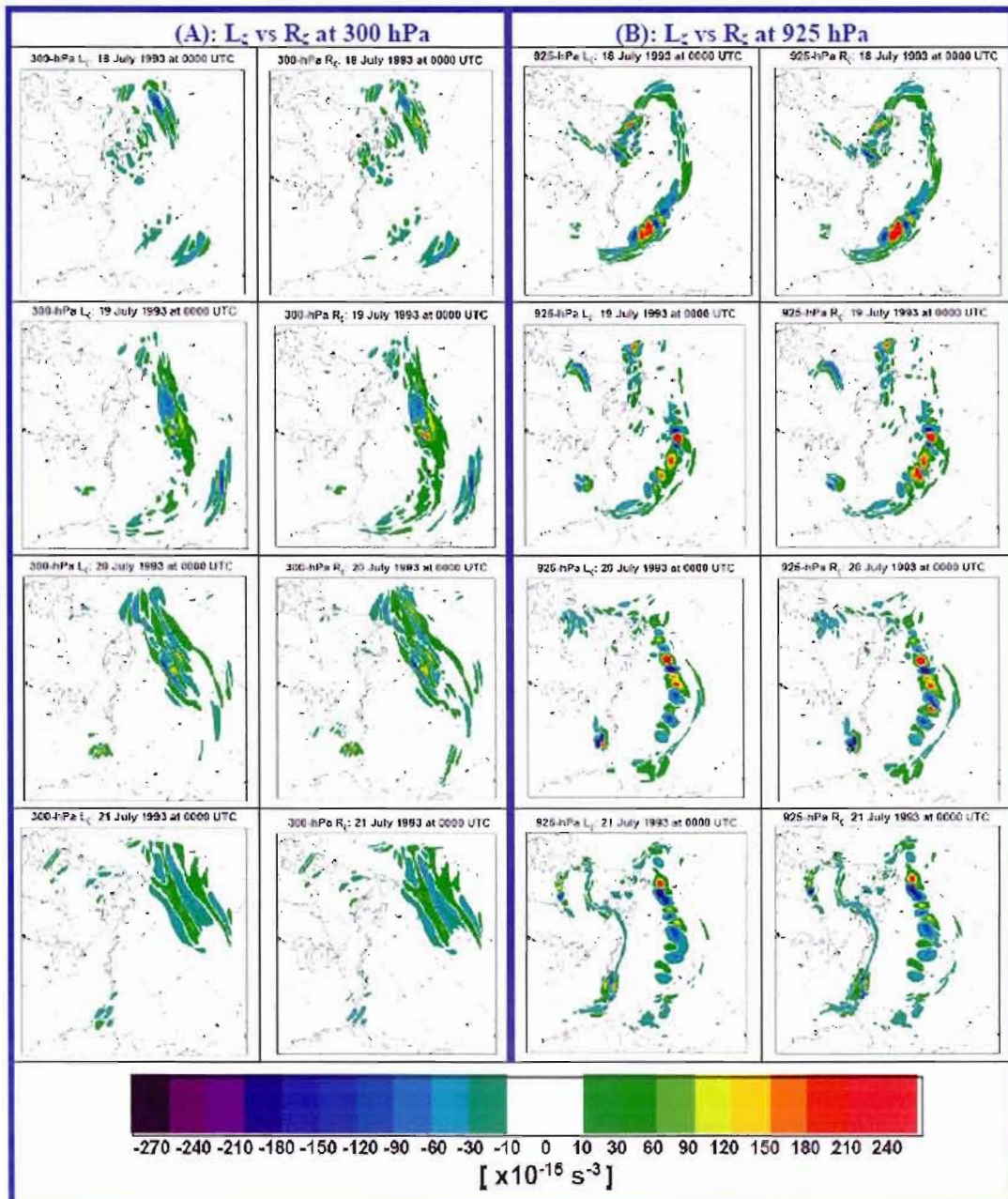


Figure 6 : Left-hand term (L_ζ) and the sum of all right-hand term (R_ζ) of the relative vorticity inter-member variance equation during the period of interest at different pressure levels: (A) 300 hPa, (B) 925 hPa.

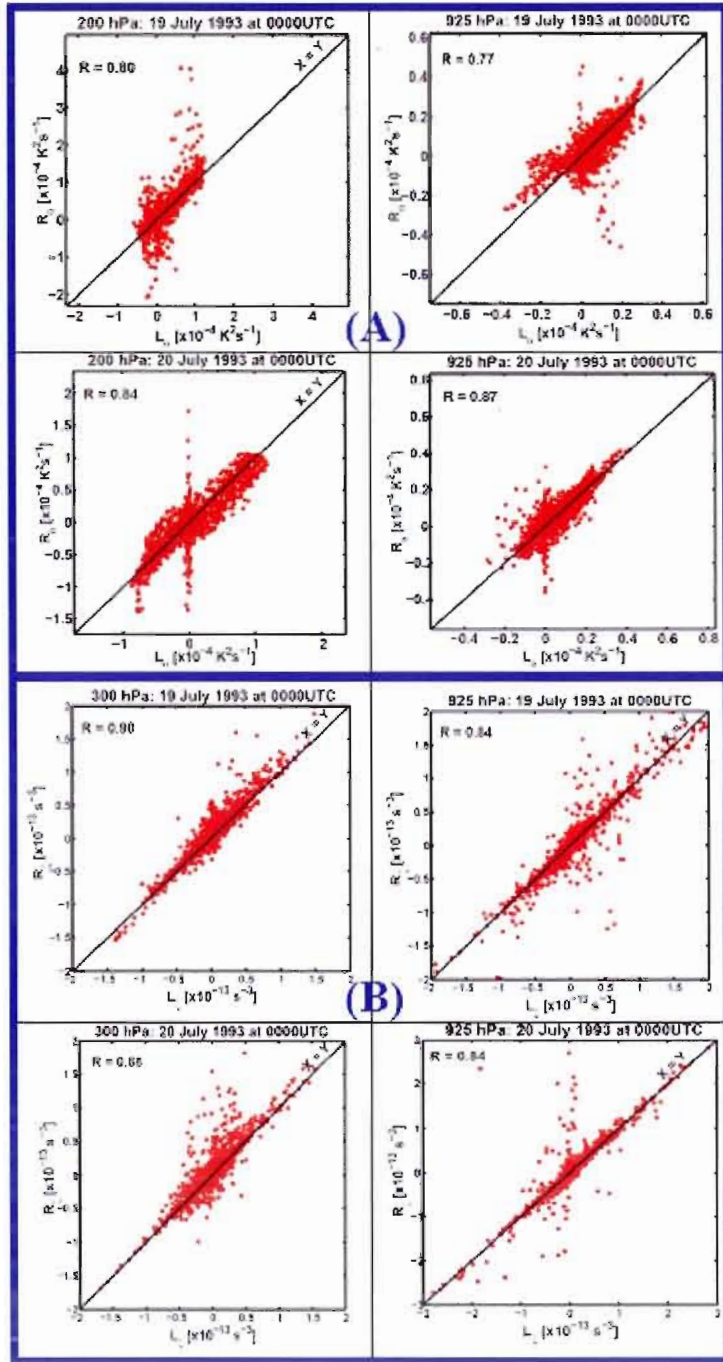


Figure 7 : Dispersion diagram of all grid points (except the sponge zone) to illustrate the comparison between the left-hand term and the sum of all right-hand terms at different pressure levels for the (A) potential temperature and the (B) relative vorticity.

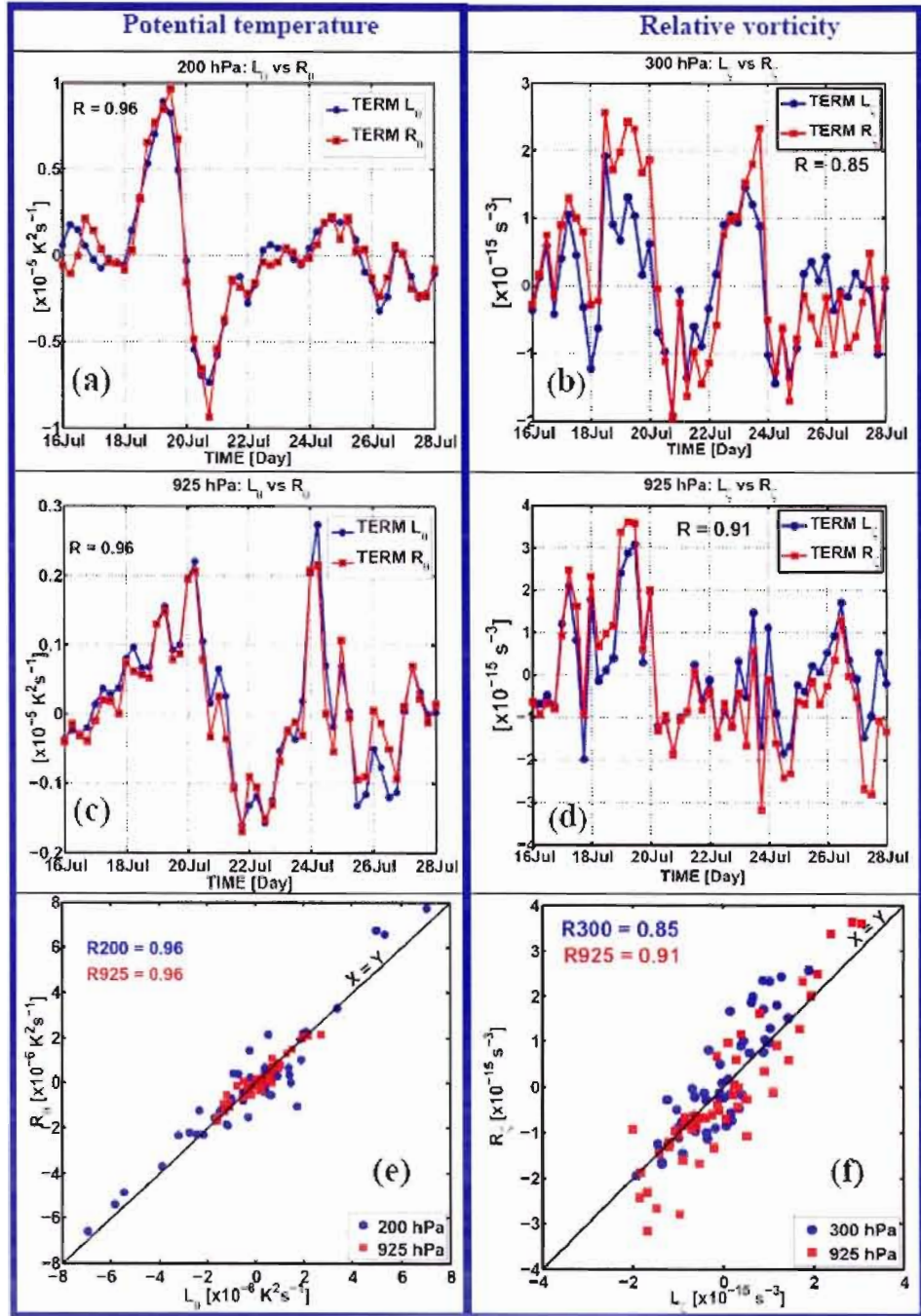


Figure 8 : Time evolution of the left-hand term and the sum of all right-hand terms of the domain-averaged inter-member variance equations for the potential temperature (a, c) and the relative vorticity (b, d) at different pressure levels; (e, f) dispersion diagram to illustrate the comparison between these two sides of the equation.

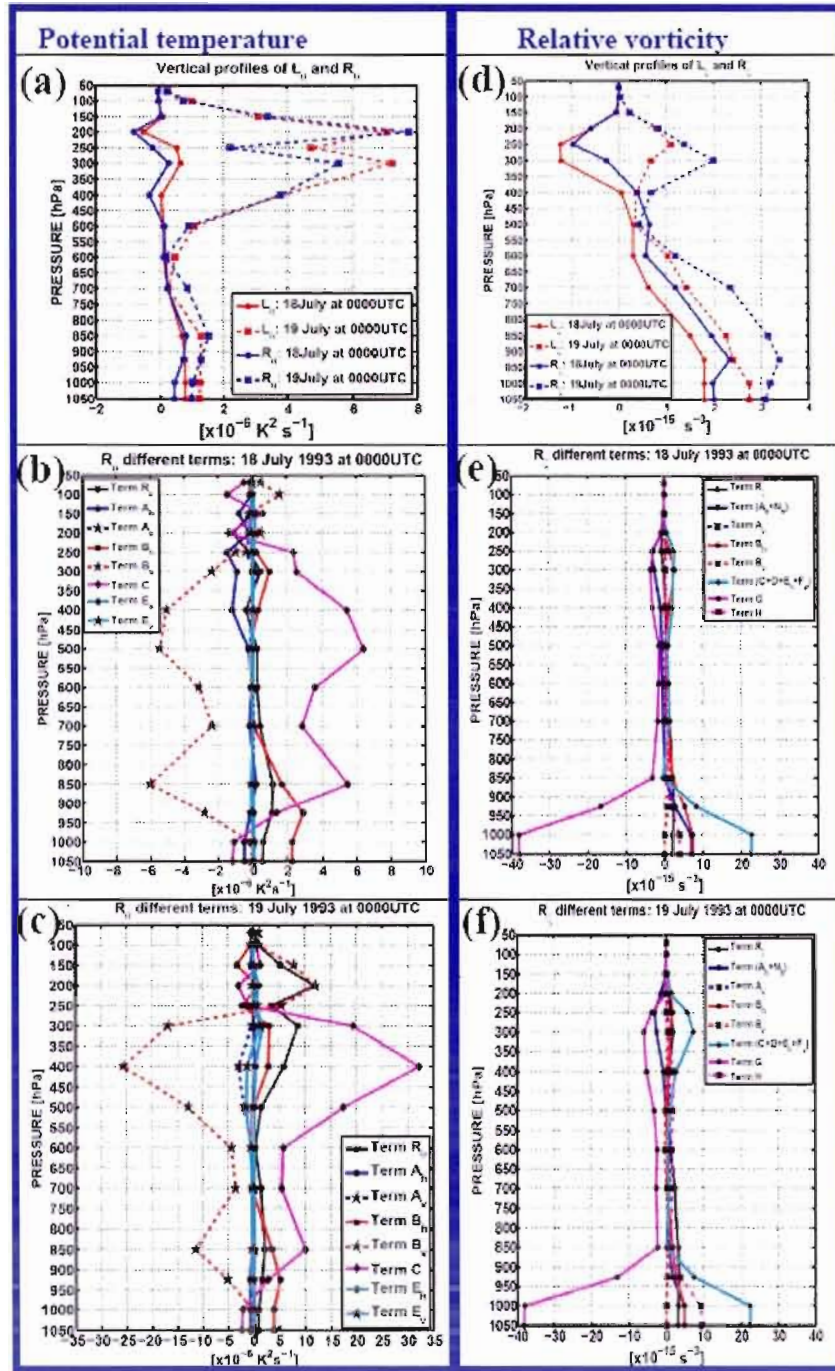


Figure 9 : Vertical profiles of R different terms of the domain-averaged inter-member variance equation for the potential temperature and the relative vorticity. The 1050-hPa level is an extrapolation of the 1000-hPa level.

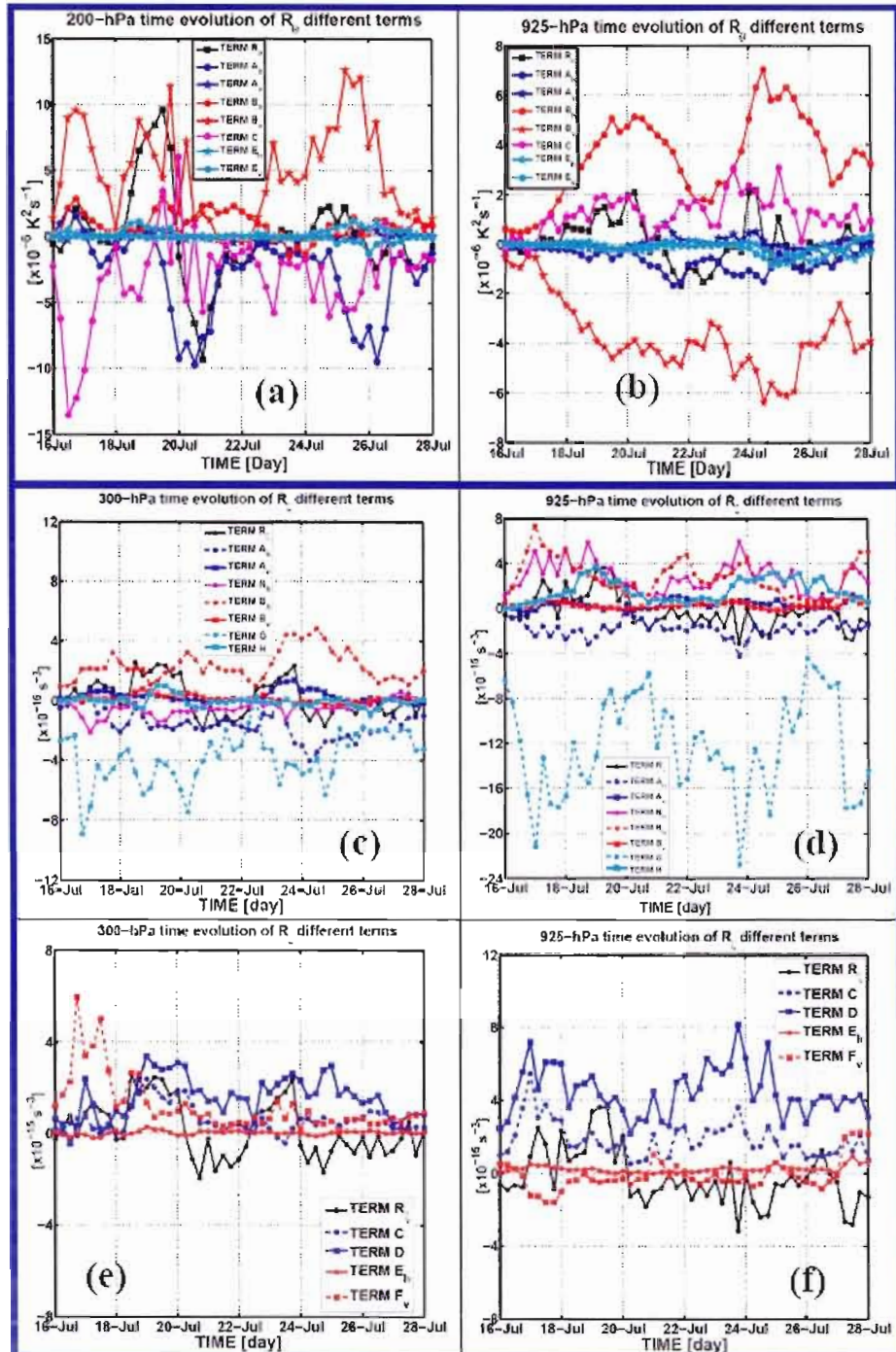


Figure 10 : Time evolution of different terms on the right-hand side of domain-averaged inter-member variance equations for the potential temperature (a, b) and the relative vorticity (c, d, e, f) during the period of interest.

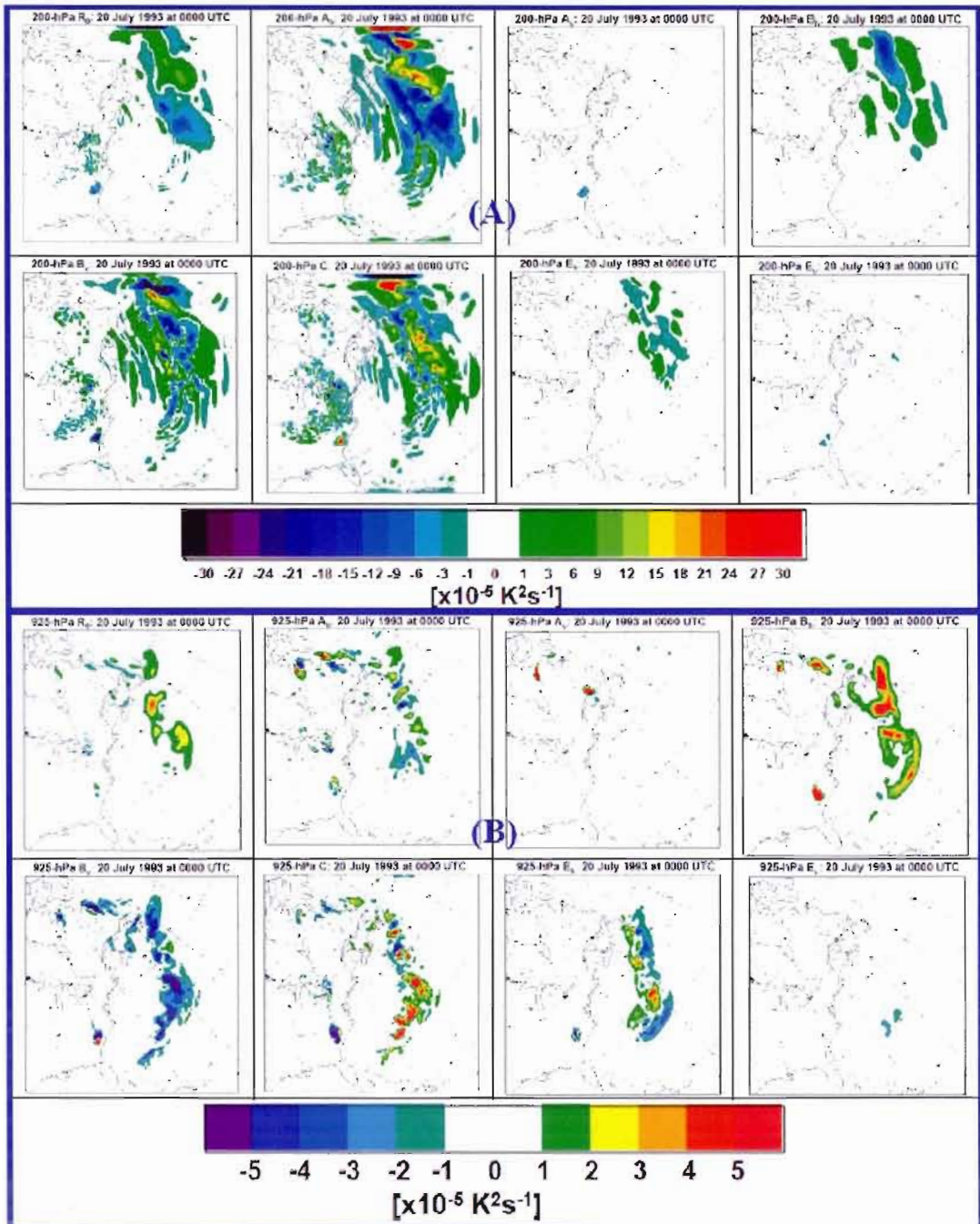


Figure 11: Field of each term on the right-hand side of the inter-member variance equation for the potential temperature on 20 July 1993 at 0000 UTC at different pressure levels: (A) 200 hPa and (B) 925 hPa.

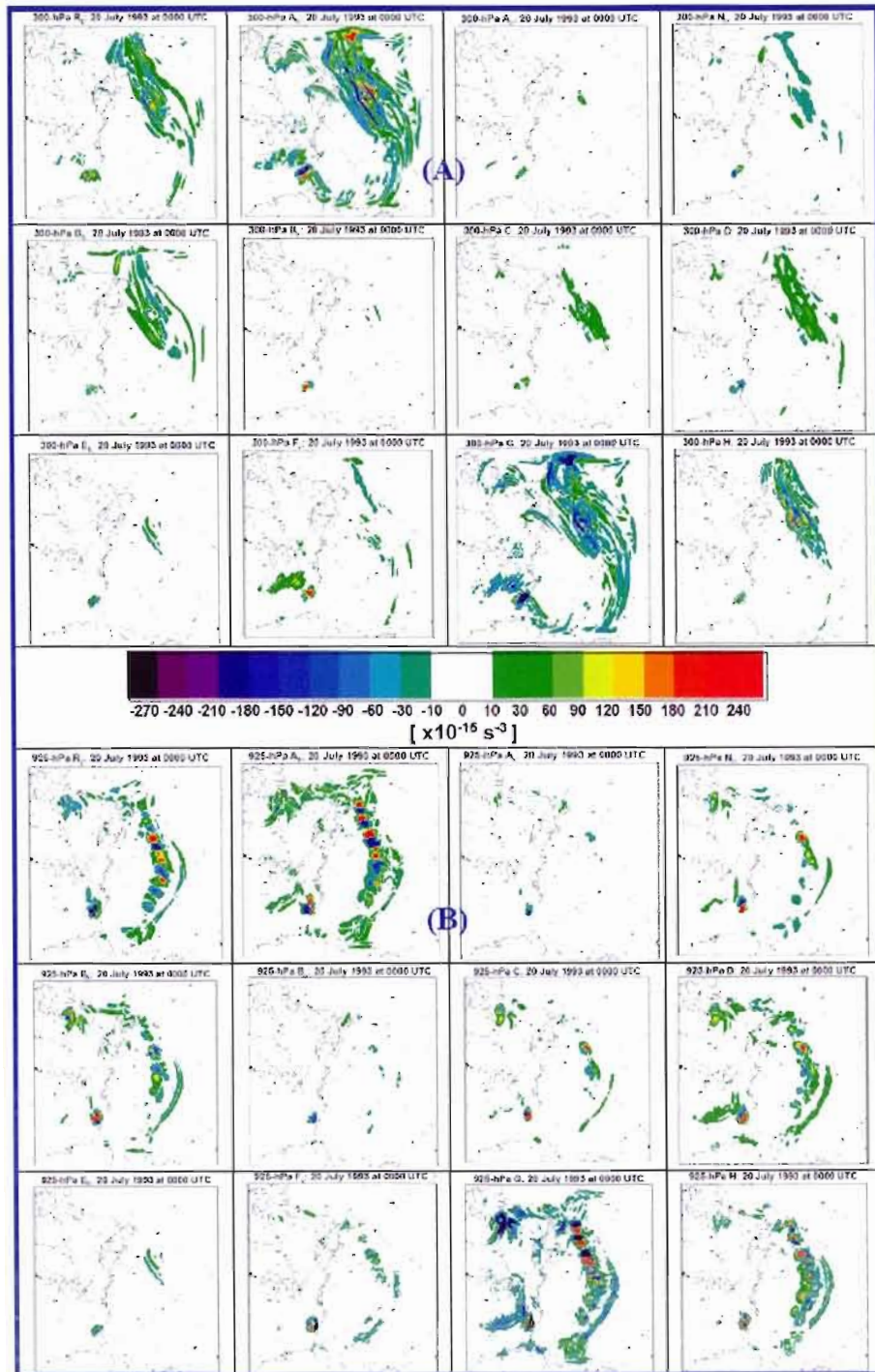


Figure 12: Fields of each term on the right-hand side of the inter-member variance equation for the relative vorticity on 20 July 1993 at different pressure levels: (A) 300 hPa, (B) 925 hPa.

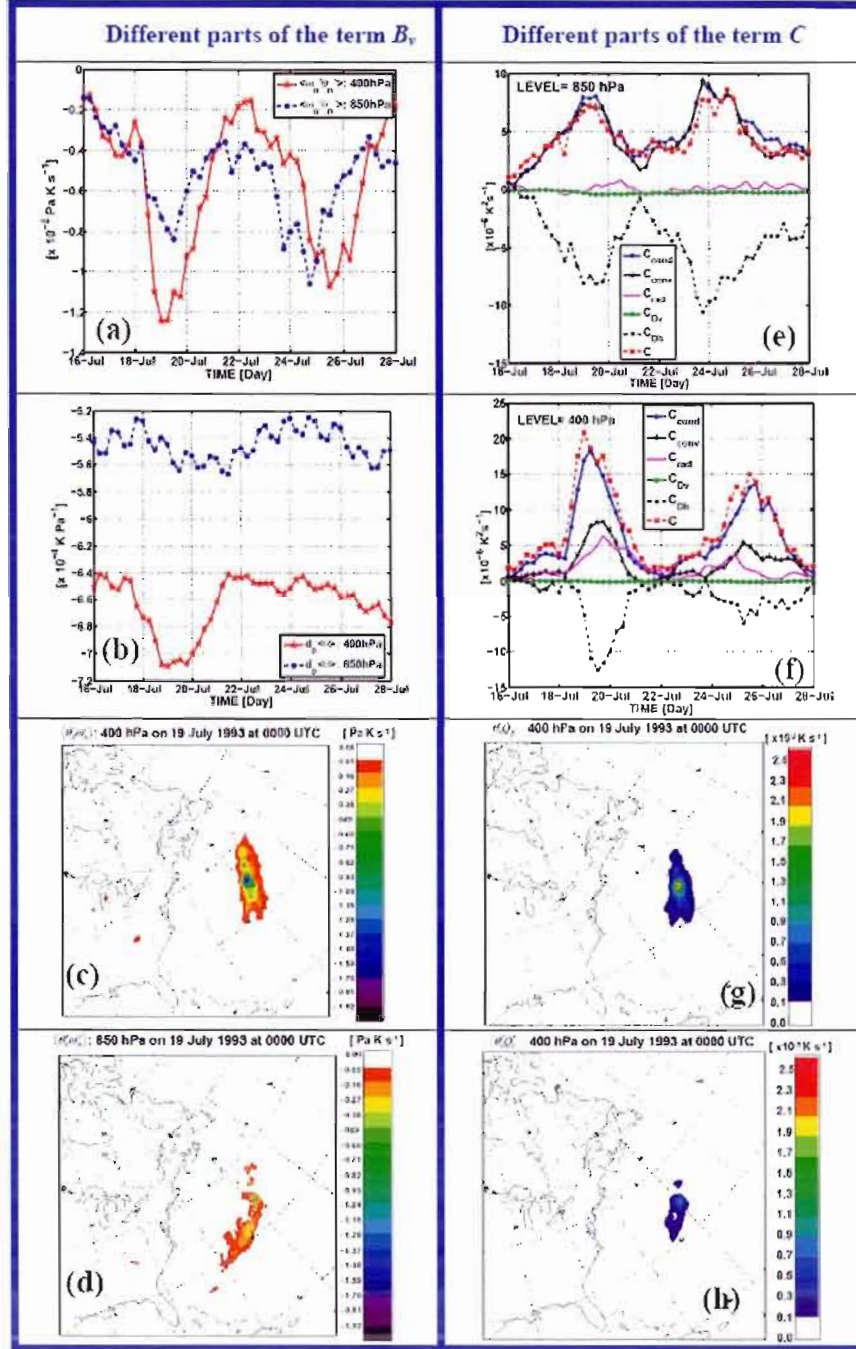


Figure 13 : Time evolution of different factors in terms B_v (a, b) and C (e, f) of the potential temperature IV equation. Different fields show the covariance of fluctuations in B_v at (c) 400 hPa and (d) 850 hPa, and the covariance of fluctuation associated to (g) condensation (precipitation) and (h) convection in C at 400 hPa. Fields are valid on July, 19 at 0000 UTC.

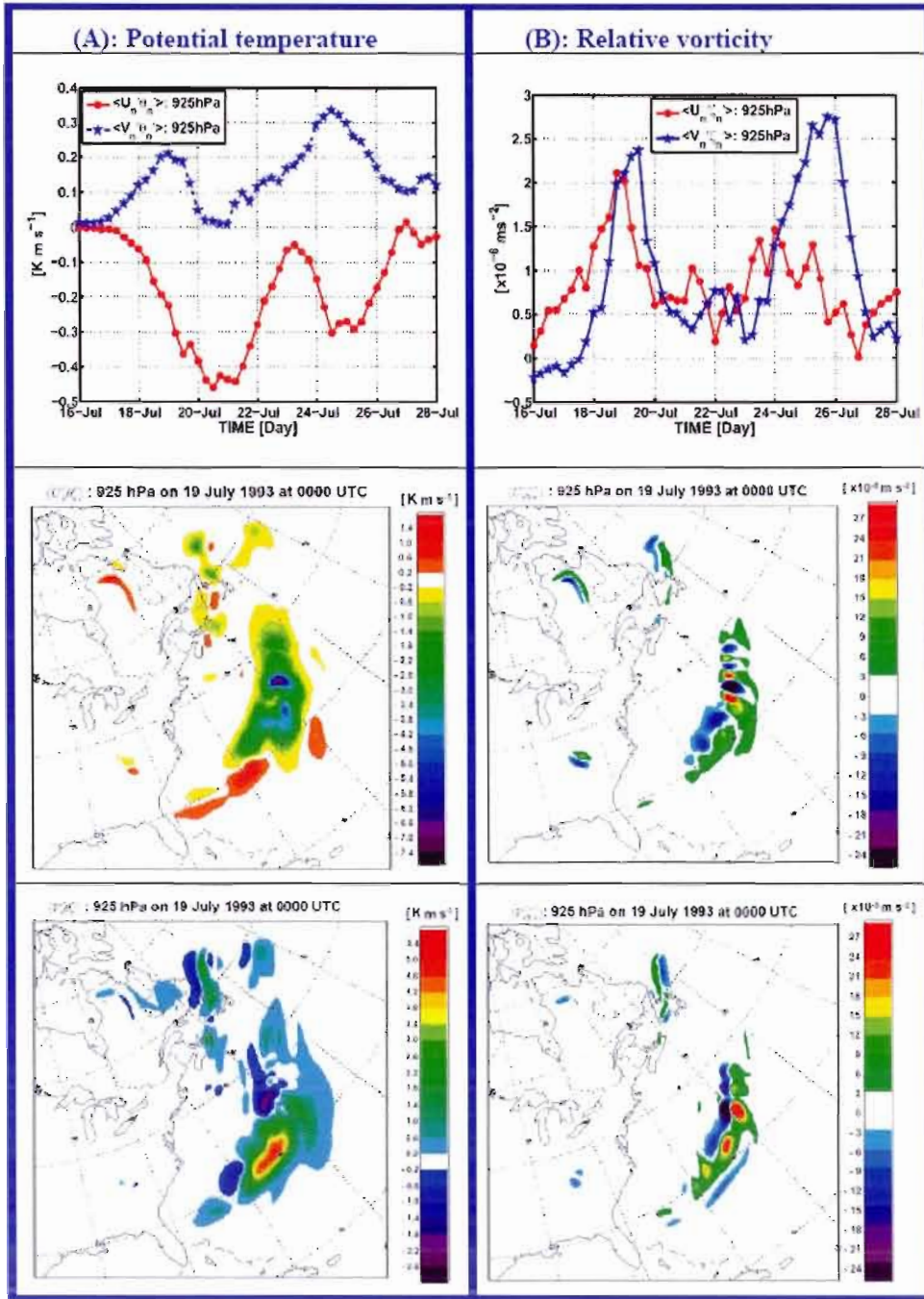


Figure 14 : Time evolution of the covariance of fluctuation in B_h of the (A) potential temperature IV equation and the (B) relative vorticity IV equation. Different fields show the covariance of fluctuations in B_h at 925 hPa on July 19, 1993 at 0000 UTC.

CONCLUSION

La variabilité interne (VI) se définit comme étant la variance inter-membres d'un ensemble de simulations qui ne diffèrent que par leurs conditions initiales (CI). Sa connaissance est importante dans l'interprétation des résultats d'un Modèle Régional du Climat puisqu'elle participe à la validation et au développement d'un modèle (Christensen et al., 2001). Plusieurs auteurs (Caya et Biner, 2004 ; Lucas-Picher et al. 2004 ; Alexandru et al. 2007 ; Lucas-Picher et al. 2008) ont étudié la VI du Modèle Régional Canadien du Climat (MRCC) à l'aide de plusieurs simulations réalisées avec différentes CI. Ils ont mis en évidence l'important de la VI du modèle dans les simulations surtout en saison estivale. En étudiant la VI sur un domaine couvrant l'Est de l'Amérique du Nord et une partie de l'océan Atlantique, Alexandru et al. (2007) ont noté des épisodes de fortes variations de la VI durant la saison d'été 1993. Le but de cette étude était d'identifier les processus physiques responsables des fortes variations de la VI en effectuant un diagnostic quantitatif des termes dynamique et diabatique.

Théoriquement, le travail a consisté à établir deux équations pronostiques de la VI pour la température potentielle et le tourbillon relatif. Concrètement, il a fallu d'abord identifier les équations résolues par le modèle pour ces deux variables atmosphériques. Puis, en considérant une réalisation de plusieurs simulations aux CI différentes, nous avons pu déterminer les équations pronostiques de la moyenne d'ensemble pour chaque variable étudiée. Ensuite, en prenant la différence des deux précédentes équations établies, nous obtenons les équations pronostiques pour la déviation par rapport à la moyenne d'ensemble. Finalement, nous aboutissons à l'équation de la variance inter-membre (ie. VI) en multipliant l'équation de la déviation par une autre quantité de déviation et en appliquant un opérateur de moyenne d'ensemble. Pour des raisons de simplicité, nous avons supposé que la variance inter-membre est la moyenne de la déviation au carré. Cette partie de l'étude a montré que la tendance de la VI (nommé L_φ : terme de gauche de l'équation)

peut être décomposée en plusieurs termes (nommé R_φ : terme de droite de l'équation) dépendant de la variable atmosphérique étudiée. Pour la température potentielle, l'équation de la VI est composée de cinq principaux termes alors que celle du tourbillon relatif est formée de 10 principaux termes. Ces deux équations présentent des termes similaires, notamment les termes relatifs au transport de la VI par l'écoulement de la moyenne d'ensemble (termes A) et les termes de covariance de fluctuations agissant sur le gradient de la moyenne d'ensemble de la variable considérée (termes B).

Dans la pratique, nous avons utilisé une base de données existante issue des travaux d'Alexandru et al. (2007) et constituée d'un ensemble de 20 simulations aux CI différentes pour analyser les résultats obtenus lors de la phase théorique de cette étude. Premièrement, nous avons analysé les caractéristiques de la VI (ie. la variance inter-membres) dans le but de comparer nos résultats à ceux d'Alexandru et al. (2007), puis de déterminer une période et une zone d'intérêts caractérisées par une importante variabilité. Ensuite, nous avons mené une étude comparative entre le terme de gauche (L_φ) et la somme de tous les termes de droite (R_φ) de l'équation afin de vérifier la validité des équations établies. Enfin, nous avons analysé la contribution des différents termes au développement et à l'évolution de la IV.

Les premiers résultats ont montré que les évolutions temporelles et les profils verticaux de la VI pour les deux variables atmosphériques étudiées sont presque similaires. Nous notons que la VI est importante dans les régions de basse et de haute troposphère, et la période du 16 au 28 juillet 1993 est marquée par une importante variation de la VI. Les maximums d'intensité sont notés aux voisinages de la tropopause (200- 300 hPa) et dans les régions de bas niveaux (925- 1000 hPa), alors que les minimums sont observés dans les régions moyennes de la troposphère (600- 700 hPa). Les champs de la moyenne saisonnière de la VI indiquent que les fortes variations sont associées aux grands événements météorologiques, comme cela a été mentionné par Alexandru et al. (2007). Selon les précédents résultats, nous nous

sommes intéressés par la suite à la période du 16 au 28 juillet et aux niveaux de forte VI (200, 300 et 925 hPa) pour analyser les résultats.

En dépit des nombreuses approximations faites pour évaluer les différents termes des équations, les résultats ont montré un bon accord quantitatif entre le terme de tendance de la VI (L_ϕ) et la somme de tous les termes de droite (R_ϕ). Les coefficients de corrélation sont supérieurs à 0,75 et peuvent même atteindre 0,90 à certains niveaux de pression. Ces résultats encourageants ont permis de mener une étude de bilan des équations pour identifier les différentes contributions à la tendance de la VI.

Les résultats révèlent que les termes dominants responsables de l'augmentation importante de la VI sont les termes de covariance impliquant les fluctuations de température potentielle et les fluctuations de chauffage diabatique, et/ou la covariance des fluctuations inter-membres agissant sur le gradient de l'état moyen. Les résultats révèlent également que les épisodes de fortes diminutions de la VI se produisent lorsque les maxima de la VI sont proches de la frontière nord-est, indiquant leur transport en dehors de la zone d'étude par l'écoulement moyen.

Pour la température potentielle, les termes dominants de l'équation bilan de la VI sont:

$$B_h = -2 \left\langle \theta'_n \bar{V}'_n \right\rangle \cdot \bar{\nabla}_h \langle \theta \rangle, \quad B_v = -2 \left\langle \theta'_n \omega'_n \right\rangle \frac{\partial \langle \theta \rangle}{\partial p} \text{ et } C = 2 \left\langle \theta'_n J'_n \right\rangle$$

Le terme C a la plus importante contribution à la tendance de la VI en raison des contributions de la convection et de la condensation à J'_n . Le terme B_v a le même ordre de grandeur que C dans la troposphère, mais de signe opposé. En effet, B_v contribue à diminuer la VI car le gradient de la moyenne d'ensemble de la température potentielle est négatif et la covariance des fluctuations de température potentielle et du mouvement vertical est également négative. Ces résultats indiquent que l'atmosphère de l'état moyen est statiquement stable et les fluctuations chaudes s'élèvent contrairement aux fluctuations froides qui descendent. Ainsi, l'énergie potentielle de la perturbation est générée par la condensation et les processus de

convection (terme C), et cette énergie est transformée en une énergie cinétique de la perturbation (terme B_v). Le terme B_h a une légère contribution positive à la tendance de la VI. En effet, le transport de chaleur par la covariance des fluctuations de température potentielle et des vents horizontaux est contre-gradient dans l'Etat de la moyenne d'ensemble. Cela correspond à une conversion de l'énergie potentielle disponible de la moyenne d'ensemble vers l'énergie potentielle disponible des fluctuations, contribuant à la croissance de la VI.

Les termes dominants de l'équation bilan de la VI pour le tourbillon relatif sont:

$$B_h = -2 \langle \zeta'_n \bar{V}'_n \rangle \cdot \bar{\nabla}_h \langle \zeta \rangle, \quad C = -2 \langle \zeta \rangle \langle \zeta'_n \bar{\nabla}_h \cdot \bar{V}'_n \rangle, \quad D = -2 \langle \zeta'_n \bar{\nabla}_h \cdot (f \bar{V}'_n) \rangle$$

$$\text{and } G = 2 \left[S \left(\left\langle \zeta'_n \left(\frac{\partial F'_{y_n}}{\partial X} - \frac{\partial F'_{x_n}}{\partial Y} \right) \right\rangle \right) - c \langle \zeta'_n \nabla^4 \zeta'_n \rangle \right]$$

Contrairement au cas de la température potentielle, nous notons que tous les termes sont associés à des composantes horizontales, ce qui suggère que la VI du tourbillon relatif est associé à l'écoulement horizontal. Le terme B_h contribue aussi à la croissance de la VI du tourbillon relatif. Cela indique que durant les épisodes de croissance importante de la VI, le transport du tourbillon relatif par covariance des fluctuations de tourbillon relatif et du vent horizontal est contre-gradient dans l'état de la moyenne d'ensemble. Les termes C et D ont aussi une contribution positive à la tendance de la VI durant les épisodes de fortes croissances, en particulier dans les bas niveaux. Cela implique que les fluctuations avec une circulation cyclonique (anticyclonique) sont liées aux fluctuations de la convergence (divergence) d'écoulement. Nous avons noté que les épisodes de forte croissance de la VI se produisent généralement lorsque l'état de la moyenne d'ensemble est cyclonique. Toutes les contributions positives à la tendance de la VI sont compensées par le terme de dissipation G , principalement à cause de la diffusion horizontale.

Pour les deux variables étudiées, les termes de transport horizontal A_h par l'écoulement de la moyenne d'ensemble ne contribuent pas à la tendance de la VI,

sauf dans les régions de grandes advection de la VI hors de la zone d'intégration, ce qui explique alors les épisodes de grande diminution de la VI. En moyenne, les termes du troisième ordre ont une faible contribution, mais elles deviennent importantes lorsque la VI est grande.

À la lumière de cette étude de bilan, nous avons pu comprendre les processus physiques responsables des variations épisodiques de la VI dans les simulations du MRCC. Toutefois, cette étude présente des limites puisqu'elle a été réalisée pour un seul régime climatique, pour un domaine situé dans les latitudes moyennes (Est de l'Amérique du Nord), pour une saison de l'année (été 1993), pour un domaine régional constitué de 120x120 points de grille avec une résolution de 45 km, et les simulations ont été réalisées avec un modèle régional piloté, le MRCC. Or il a été montré que la VI peut varier considérablement suivant le régime climatique, la saison et la taille du domaine. Donc, des études similaires devraient être envisagées pour des configurations différentes et pour des régimes climatiques différents afin de généraliser les conclusions de la présente étude.

APPENDICES

Appendix A – Reynolds Averaging and Rules of Averaging

Considering two variables f and g that are split into ensemble-mean and deviation parts:

$$\begin{aligned} f &= \langle f \rangle + f' \\ g &= \langle g \rangle + g' \end{aligned} \quad \text{A-1}$$

Reynolds decomposition of the product gives:

$$fg = \langle f \rangle \langle g \rangle + f' \langle g \rangle + \langle f \rangle g' + f' g' \quad \text{A-2}$$

so that,

$$\langle fg \rangle = \langle f \rangle \langle g \rangle + \langle f' g' \rangle \quad \text{A-3}$$

and so,

$$fg - \langle fg \rangle = f' \langle g \rangle + \langle f \rangle g' + f' g' - \langle f' g' \rangle \quad \text{A-4}$$

The following results from A-1:

$$\begin{aligned} \langle f' \rangle &= 0; \\ \langle \langle f \rangle g \rangle &= \langle f \rangle \langle g \rangle; \\ \langle f + g \rangle &= \langle f \rangle + \langle g \rangle \end{aligned} \quad \text{A-5}$$

If α is a constant, we also get;

$$\langle \alpha f \rangle = \alpha \langle f \rangle \quad \text{A-6}$$

From the definition of partial derivatives:

$$\left\langle \frac{\partial f}{\partial \xi} \right\rangle = \frac{\partial \langle f \rangle}{\partial \xi} \quad \text{A-7}$$

where ξ represent space or time variable.

Appendix B- Relative vorticity equation ζ for the polar stereographic and the vertical pressure coordinates

Consider a system of the polar stereographic projection (X, Y) and the vertical pressure coordinates, the Euler equations, with the meteorological “traditional” approximation, take the following form:

$$\frac{\partial U}{\partial t} + \vec{V} \cdot \vec{\nabla} U + \omega \frac{\partial U}{\partial p} = fV - K \frac{\partial S}{\partial X} - \frac{\partial \phi}{\partial X} + F_x - c \nabla^4 U \quad \text{B-1}$$

$$\frac{\partial V}{\partial t} + \vec{V} \cdot \vec{\nabla} V + \omega \frac{\partial V}{\partial p} = -fU - K \frac{\partial S}{\partial Y} - \frac{\partial \phi}{\partial Y} + F_y - c \nabla^4 V \quad \text{B-2}$$

where the different variables of these equations are defined as:

- $$\begin{pmatrix} dX \\ dY \end{pmatrix} = m \times \begin{bmatrix} -\sin \lambda & -\cos \lambda \\ \cos \lambda & -\sin \lambda \end{bmatrix} \begin{pmatrix} dx \\ dy \end{pmatrix}$$

with λ the longitude and (x, y) the local horizontal Cartesian coordinate system.

- $K = (U^2 + V^2)/2$ and $S = m^2$ with $m = (1 + \sin \varphi_0)/(1 + \sin \varphi)$ the map scale factor, where φ is the latitude and φ_0 the latitude at which the plane of projection intersects the sphere.
- (F_x, F_y) correspond to components of sources or sinks of momentum. These two components include surface friction, vertical diffusion and gravity wave drag. The last term of equations (B-1) and (B-2) takes into account the horizontal diffusion to parameterise the cascade of information to unresolved scale, where the constant of diffusion c for the 45-km version of the CRCM is $c = 1.85 \cdot 10^{13} \text{ m}^4 \text{s}^{-1}$ (Laprise et al. 1998).
- $f = 2\Omega \sin \varphi$ is the Coriolis parameter.

By adding and subtracting to equations B-1 and B-2 these two expressions: $SV[\partial V/\partial X]$ and $SU[\partial U/\partial Y]$ respectively, we obtain:

$$\frac{\partial U}{\partial t} + \bar{V} \cdot \bar{\nabla} U + \omega \frac{\partial U}{\partial p} = (\zeta + f)V - \frac{\partial(KS)}{\partial X} - \frac{\partial \phi}{\partial X} + F_x - c\nabla^4 U \quad \text{B-3}$$

$$\frac{\partial V}{\partial t} + \bar{V} \cdot \bar{\nabla} V + \omega \frac{\partial V}{\partial p} = -(\zeta + f)U - \frac{\partial(KS)}{\partial Y} - \frac{\partial \phi}{\partial Y} + F_y - c\nabla^4 V \quad \text{B-4}$$

where $\zeta = S \left[\frac{\partial V}{\partial X} - \frac{\partial U}{\partial Y} \right]$ is the relative vorticity expression.

Applying $S \times \left[\frac{\partial(B-2)}{\partial X} - \frac{\partial(B-1)}{\partial Y} \right]$, we obtain the relative vorticity equation:

$$\frac{\partial \zeta}{\partial t} + \bar{V} \cdot (\zeta \bar{V}) + \omega \frac{\partial \zeta}{\partial p} = -\bar{V} \cdot (f \bar{V}) + S \left[\frac{\partial \omega}{\partial Y} \frac{\partial U}{\partial p} - \frac{\partial \omega}{\partial X} \frac{\partial V}{\partial p} \right] + S \left[\frac{\partial F_y}{\partial X} - \frac{\partial F_x}{\partial Y} \right] - c\nabla^4 \zeta \quad \text{B-5}$$

Using the fact that the Coriolis parameter does not depends on time and pressure, the absolute vorticity (η) equation may be written as:

$$\frac{\partial \eta}{\partial t} + \bar{V} \cdot (\eta \bar{V}) + \omega \frac{\partial \eta}{\partial p} = S \left[\frac{\partial \omega}{\partial Y} \frac{\partial U}{\partial p} - \frac{\partial \omega}{\partial X} \frac{\partial V}{\partial p} \right] + S \left[\frac{\partial F_y}{\partial X} - \frac{\partial F_x}{\partial Y} \right] - c\nabla^4 \zeta \quad \text{B-6}$$

where $\eta = \zeta + f$

Appendix C – Spatial and temporal finite differencing

To derive second-order finite-difference equations, the following sum and difference operations are defined (e.g. Haltiner and Williams 1980; Durran 1998):

$$\delta_t F(i, j, k, t) \equiv \frac{F(i, j, k, t+1) - F(i, j, k, t-1)}{2\Delta t} \quad \text{C-1}$$

$$\overline{F(i, j, k, t)}^x \equiv \frac{F(i+1/2, j, k, t) + F(i-1/2, j, k, t)}{2} \quad \text{C-2}$$

$$\overline{F(i, j, k, t)}^y \equiv \frac{F(i, j+1/2, k, t) + F(i, j-1/2, k, t)}{2}$$

$$\delta_x F(i, j, k, t) \equiv \frac{F(i+1/2, j, k, t) - F(i-1/2, j, k, t)}{\Delta X} \quad \text{C-3}$$

$$\delta_y F(i, j, k, t) \equiv \frac{F(i, j+1/2, k, t) - F(i, j-1/2, k, t)}{\Delta Y}$$

$$\delta_x \overline{F(i, j, k, t)}^x \equiv \frac{F(i+1, j, k, t) - F(i-1, j, k, t)}{2\Delta X} \quad \text{C-4}$$

$$\delta_y \overline{F(i, j, k, t)}^y \equiv \frac{F(i, j+1, k, t) - F(i, j-1, k, t)}{2\Delta Y}$$

$$\delta_p F(i, j, k, t) \equiv \frac{F(i, j, k+1, t) - F(i, j, k-1, t)}{p(k+1) - p(k-1)} \quad \text{C-5}$$

$$\nabla \cdot \vec{V} \approx S \left[\delta_x \overline{U}^x + \delta_y \overline{V}^y \right] \quad \text{where} \quad \vec{V} \equiv (U, V) \quad \text{C-6}$$

Appendix D – Different terms of the IV prognostic equation for the relative vorticity

$$L_\zeta(i, j, k, t) = R_\zeta(i, j, k, t) \quad \text{D-1}$$

where,

$$\begin{aligned} L_\zeta(i, j, k, t) &\approx \delta_t \sigma_\zeta^2(i, j, k, t) \\ &\approx \frac{\sigma_\zeta^2(i, j, k, t+1) - \sigma_\zeta^2(i, j, k, t-1)}{2\Delta t} \end{aligned} \quad \text{D-2}$$

and,

$$R_\zeta(i, j, k, t) = [A_h + A_v + N_h + B_h + B_v + C + D + E_h + F_v + G + H](i, j, k, t) \quad \text{D-3}$$

with

$$\begin{aligned} A_h &\approx -S \left[\delta_x \left(\overline{\langle U \rangle^x} \overline{\sigma_\zeta^2}^x \right) + \delta_y \left(\overline{\langle V \rangle^y} \overline{\sigma_\zeta^2}^y \right) \right]; \quad A_v \approx -\delta_\rho (\langle \omega \rangle \sigma_\zeta^2) \\ N_h &\approx -2S \sigma_i^2 \left[\delta_x \overline{\langle U \rangle^x} + \delta_y \overline{\langle V \rangle^y} \right]; \\ B_h &\approx -2S \left[\langle \zeta'_n U'_n \rangle \delta_x \overline{\langle \theta \rangle^x} + \langle \zeta'_n V'_n \rangle \delta_y \overline{\langle \zeta \rangle^y} \right]; \quad B_v \approx -2 \langle \zeta'_n \omega'_n \rangle \delta_\rho \langle \zeta \rangle \\ C &\approx -2S \langle \zeta \rangle \left[\left\langle \zeta'_n \delta_x \overline{U'_n}^x \right\rangle + \left\langle \zeta'_n \delta_y \overline{V'_n}^y \right\rangle \right]; \\ D &\approx -2S \left[\left\langle \zeta'_n \delta_x \left(\overline{f}^x \overline{U'_n}^x \right) \right\rangle + \left\langle \zeta'_n \delta_y \left(\overline{f}^y \overline{V'_n}^y \right) \right\rangle \right]; \\ E_h &\approx 2S \left[\delta_y \overline{\langle \omega \rangle^y} \left\langle \zeta'_n \delta_\rho U'_n \right\rangle - \delta_x \overline{\langle \omega \rangle^x} \left\langle \zeta'_n \delta_\rho V'_n \right\rangle \right]; \\ F_v &\approx 2S \left[\left\langle \zeta'_n \delta_y \overline{\omega'_n}^y \right\rangle \delta_\rho \langle U \rangle - \left\langle \zeta'_n \delta_x \overline{\omega'_n}^x \right\rangle \delta_\rho \langle V \rangle \right]; \end{aligned} \quad \text{D-4}$$

$$\begin{aligned}
G \approx & 2 \left[S \left(\left\langle \zeta'_n \delta_X \overline{F'}^X_{Y_n} \right\rangle - \left\langle \zeta'_n \delta_Y \overline{F'}^Y_{X_n} \right\rangle \right) - c \left\langle \zeta'_n \nabla^4 \zeta'_n \right\rangle \right]; \\
H \approx & -2S \left[\left\langle \zeta'_n \delta_X \left(\overline{\zeta'}^X_n \overline{U'}^X_n \right) \right\rangle + \left\langle \zeta'_n \delta_X \left(\overline{\zeta'}^X_n \overline{V'}^X_n \right) \right\rangle \right] - \left\langle \omega'_n \delta_p \zeta'^2_n \right\rangle \\
& + 2S \left[\left\langle \zeta'_n \delta_Y \overline{\omega'}^Y_n \delta_p U'_n \right\rangle - \left\langle \zeta'_n \delta_X \overline{\omega'}^X_n \delta_p V'_n \right\rangle \right]
\end{aligned}$$

Appendix E – Assessment of the vertical motion: ω_n ($\equiv \frac{dp}{dt}$)

By definition, the vertical velocity can be written in this form:

$$w = \frac{dz}{dt} = \frac{1}{g} \frac{d\phi}{dt} \quad \text{E-1}$$

where $\phi = gz$ represents the geopotential height. Expanding the total derivative into its components gives

$$w = \frac{1}{g} \left[\frac{\partial \phi}{\partial t} \Big|_p + \bar{V}_h \cdot \nabla_p \phi + \omega \frac{\partial \phi}{\partial p} \right] \quad \text{E-2}$$

Using the hydrostatic equation, we can write: $\frac{\partial \phi}{\partial p} = -\frac{RT}{p}$, so

$$\omega = \frac{p}{RT} \left[\frac{\partial \phi}{\partial t} \Big|_p + \bar{V}_h \cdot \nabla_p \phi - gw \right] \quad \text{E-3}$$

All variables in this last equation are archived as the CRCM output data. Thus, the vertical motion is assessed as follow:

$$\omega \approx \frac{p}{RT} \left[\delta_t \phi + S \left(U \delta_x \bar{\phi}^x + V \delta_y \bar{\phi}^y \right) - gw \right] \quad \text{E-4}$$

Thus, the vertical motion for the member n is written as:

$$\omega_n \approx \frac{p}{RT_n} \left[\delta_t \phi_n + S \left(U_n \delta_x \bar{\phi}_n^x + V_n \delta_y \bar{\phi}_n^y \right) - gw_n \right] \quad \text{E-5}$$

Appendix F – The absolute vorticity IV equation

In the horizontal polar stereographic and the isobaric coordinates (X, Y, p) , the absolute vorticity ($\eta_n = \zeta_n + f$) equation (see details in the Appendix B) for each member can be written as:

$$\frac{d\eta_n}{dt} \equiv \frac{\partial \eta_n}{\partial t} + \bar{\nabla} \cdot (\eta_n \bar{V}_n) + \omega_n \frac{\partial \eta_n}{\partial p} = S \left[\frac{\partial \omega_n}{\partial Y} \frac{\partial U_n}{\partial p} - \frac{\partial \omega_n}{\partial X} \frac{\partial V_n}{\partial p} \right] + S \left[\frac{\partial F_{Yn}}{\partial X} - \frac{\partial F_{Xn}}{\partial Y} \right] - c \nabla^4 \zeta_n \quad \text{F-1}$$

By using similar steps as described in the section 2.2, the ensemble-mean and deviation equations of absolute vorticity are written as:

$$\frac{\partial \langle \eta \rangle}{\partial t} + \bar{\nabla} \cdot \langle \bar{V} \eta \rangle + \left\langle \omega \frac{\partial \eta}{\partial p} \right\rangle = S \left[\left\langle \frac{\partial \omega}{\partial Y} \frac{\partial U}{\partial p} \right\rangle - \left\langle \frac{\partial \omega}{\partial X} \frac{\partial V}{\partial p} \right\rangle \right] + S \left[\frac{\partial \langle F_Y \rangle}{\partial X} - \frac{\partial \langle F_X \rangle}{\partial Y} \right] - c \nabla^4 \langle \zeta \rangle \quad \text{F-2}$$

and

$$\begin{aligned} \frac{D\eta'_n}{Dt} &\equiv \frac{\partial \eta'_n}{\partial t} + \langle \bar{V} \rangle \cdot \bar{\nabla} \eta'_n + \langle \omega \rangle \frac{\partial \eta'_n}{\partial p} = -\eta'_n \bar{\nabla} \cdot \langle \bar{V} \rangle - \bar{V}'_n \cdot \bar{\nabla} \langle \eta \rangle - \omega'_n \frac{\partial \langle \eta \rangle}{\partial p} - \langle \eta \rangle \bar{\nabla} \cdot \bar{V}'_n - \bar{\nabla} \cdot (\eta'_n \bar{V}'_n) - \omega'_n \frac{\partial \eta'_n}{\partial p} \\ &+ \bar{\nabla} \cdot \langle \eta'_n \bar{V}'_n \rangle + \left\langle \omega'_n \frac{\partial \eta'_n}{\partial p} \right\rangle + S \left[\frac{\partial \langle \omega \rangle}{\partial Y} \frac{\partial U'_n}{\partial p} - \frac{\partial \langle \omega \rangle}{\partial X} \frac{\partial V'_n}{\partial p} \right] + S \left[\frac{\partial \omega'_n}{\partial Y} \frac{\partial \langle U \rangle}{\partial p} - \frac{\partial \omega'_n}{\partial X} \frac{\partial \langle V \rangle}{\partial p} \right] \quad \text{F-3} \\ &+ S \left[\frac{\partial \omega'_n}{\partial Y} \frac{\partial U'_n}{\partial p} - \frac{\partial \omega'_n}{\partial X} \frac{\partial V'_n}{\partial p} \right] + S \left[\left\langle \frac{\partial \omega'_n}{\partial X} \frac{\partial V'_n}{\partial p} \right\rangle - \left\langle \frac{\partial \omega'_n}{\partial Y} \frac{\partial U'_n}{\partial p} \right\rangle \right] + S \left[\frac{\partial F'_{Yn}}{\partial X} - \frac{\partial F'_{Xn}}{\partial Y} \right] - c \nabla^4 \zeta'_n \end{aligned}$$

The inter-member variance equation for absolute vorticity (σ_η^2) is obtained by

applying $\langle \eta'_n \times (\text{F-3}) \rangle$, to get:

$$\begin{aligned} \frac{1}{2} \frac{D\sigma_\eta^2}{Dt} &\equiv \frac{\partial}{\partial t} \left(\frac{\sigma_\eta^2}{2} \right) + \frac{\langle \bar{V} \rangle}{2} \cdot \bar{\nabla} \sigma_\eta^2 + \frac{\langle \omega \rangle}{2} \frac{\partial \sigma_\eta^2}{\partial p} = -\sigma_\eta^2 \bar{\nabla} \cdot \langle \bar{V} \rangle - \langle \eta'_n \bar{V}'_n \rangle \cdot \bar{\nabla} \langle \eta \rangle - \langle \eta'_n \omega'_n \rangle \frac{\partial \langle \eta \rangle}{\partial p} - \langle \eta \rangle \langle \eta'_n \bar{\nabla} \cdot \bar{V}'_n \rangle \\ &S \left[\frac{\partial \langle \omega \rangle}{\partial Y} \left\langle \eta'_n \frac{\partial U'_n}{\partial p} \right\rangle - \frac{\partial \langle \omega \rangle}{\partial X} \left\langle \eta'_n \frac{\partial V'_n}{\partial p} \right\rangle \right] + S \left[\left\langle \eta'_n \frac{\partial \omega'_n}{\partial Y} \right\rangle \frac{\partial \langle U \rangle}{\partial p} - \left\langle \eta'_n \frac{\partial \omega'_n}{\partial X} \right\rangle \frac{\partial \langle V \rangle}{\partial p} \right] \\ &+ S \left[\left\langle \eta'_n \frac{\partial F'_{Yn}}{\partial X} \right\rangle - \left\langle \eta'_n \frac{\partial F'_{Xn}}{\partial Y} \right\rangle \right] - c \underbrace{\left\langle \eta'_n \nabla^4 \zeta'_n \right\rangle - \left\langle \eta'_n \bar{\nabla} \cdot (\eta'_n \bar{V}'_n) \right\rangle}_{3^{rd} \text{ order}} - \underbrace{\left\langle \frac{\omega'_n}{2} \frac{\partial \eta'^2}{\partial p} \right\rangle + S \left[\left\langle \eta'_n \frac{\partial \omega'_n}{\partial Y} \frac{\partial U'_n}{\partial p} \right\rangle - \left\langle \eta'_n \frac{\partial \omega'_n}{\partial X} \frac{\partial V'_n}{\partial p} \right\rangle \right]}_{3^{rd} \text{ order}} \quad \text{F-4} \end{aligned}$$

where: $\sigma_\eta^2 = \langle \eta'^2 \rangle$

RÉFÉRENCES

- Alexandru A, de Elia R, Laprise R (2007) Internal Variability in regional climate downscaling at the seasonal scale. *Mon Weather Rev* 135:3221-3238
- Caya D, Biner S (2004) Internal Variability of RCM Simulations over an Annual Cycle. *Clim Dyn* 22:33-46
- Caya D, Laprise R (1999) A semi-implicit semi-Lagrangian regional climate model: The Canadian RCM. *Mon Weather Rev* 127:341-362
- Christensen OB, Gaertner MA, Prego JA, Polcher J (2001) Internal variability of regional climate models. *Clim Dyn* 17:875-887
- Duran DR (1998) Numerical methods for wave equations in geophysical fluid dynamics. Ed Springer-Verl, 482 pp
- Gal-Chen T, Sommerville RCJ (1975) On the use of a Coordinate transformation for the Solution of the Navier-Stokes Equations. *J Comput Phys* 17:209-228
- Giorgi F, Bi X (2000) A study of internal variability of regional climate model. *J Geophys Res* 105:29503-29521
- Haltiner GJ, Williams RT (1980) Numerical prediction and dynamic meteorology. Ed John Wiley & Son, 477 pp
- Laprise R, Caya D, Giguère M, Bergeron G, Côté H, Blanchet J-P, Boer GJ, McFarlane N (1998) Climate and Climate Change in Western Canada as Simulated by the Canadian Regional Climate Model. *Atmos-Ocean* 36:119-167
- Lorenz EN (1955) Available potential energy and the maintenance of the general circulation. *Tellus* 7:157-167
- Lorenz EN (1963) Deterministic nonperiodic flow. *J Atmos Sci* 20:130-141
- Lorenz EN (1967) The nature and theory of the general circulation of the atmosphere. *World Meteorological Organ* 218 TP 115 161 pp
- Lucas-Picher P, Caya D, Biner S, (2004) RCM's internal variability as function of domain size. *Research Activities in Atmospheric and Oceanic Modelling*, WMO/TD, J Côté Ed, 1220 34:7.27-7.28

- Lucas-Picher P, Caya D, de Elia R, Laprise R (2008) Investigation of regional climate models' internal variability with a ten-member ensemble of 10-year simulations over a large domain. *Clim Dyn* doi:10.1007/s00382-008-0384-8
- Rinke A, Dethloff K (2000) On the sensitivity of a regional Arctic climate model to initial and boundary conditions. *Clim Res* 14:101-113
- Rinke A, Marbaix P, Dethloff K (2004) Internal variability in Arctic regional climate simulations: case study for the Sheba year. *Clim Res* 27:197-209
- Weisse R, Heyen H, von Storch H (2000) Sensitivity of a regional atmospheric model to a sea state dependent roughness and the need of ensemble calculations. *Mon Weather Rev* 128:3631-3642